© 2014. Published by The Company of Biologists Ltd | Development (2014) 141, 307-317 doi:10.1242/dev.096107

RESEARCH ARTICLE

# Notch3 establishes brain vascular integrity by regulating pericyte number

**Yuying Wang[1], Luyuan Pan[2], Cecilia B. Moens[2] and Bruce Appel[1,*]**

## ABSTRACT

Brain pericytes are important regulators of brain vascular integrity, permeability and blood flow. Deficiencies of brain pericytes are associated with neonatal intracranial hemorrhage in human fetuses, as well as stroke and neurodegeneration in adults. Despite the important functions of brain pericytes, the mechanisms underlying their development are not well understood and little is known about how pericyte density is regulated across the brain. The Notch signaling pathway has been implicated in pericyte development, but its exact roles remain ill defined. Here, we report an investigation of the Notch3 receptor using zebrafish as a model system. We show that zebrafish brain pericytes express *notch3* and that *notch3* mutant zebrafish have a deficit of brain pericytes and impaired blood-brain barrier function. Conditional loss- and gain-of-function experiments provide evidence that Notch3 signaling positively regulates brain pericyte proliferation. These findings establish a new role for Notch signaling in brain vascular development whereby Notch3 signaling promotes expansion of the brain pericyte population.

**KEY WORDS: Pericytes, Notch3, Blood-brain barrier, Intraventricular hemorrhage, Vasculature**

## INTRODUCTION

The vertebrate vascular wall is composed of two major cell types, endothelial cells (ECs) and mural cells, which envelop the ECs. When associated with large arteries and veins, mural cells are multi-layered and referred to as vascular smooth muscle cells (vSMCs). When associated with capillaries, mural cells appear as sparse solitary cells and are referred to as pericytes. Until recently, mural cells were viewed as stationary cells that structurally support the vascular wall. However, they are now recognized as dynamic regulators of vascular development and homeostasis (Armulik et al., 2011; Bell et al., 2010; Lindahl et al., 1997; von Tell et al., 2006). Brain pericytes, in particular, regulate key aspects of cerebral vascular function. Recent studies using pericyte-deficient mouse models resulting from defective platelet-derived growth factor (PDGF) signaling demonstrated that brain pericytes are required for blood-brain barrier (BBB) function during development (Armulik et al., 2010; Daneman et al., 2010). Brain pericytes have been also shown to regulate capillary diameter in response to neural activity (Peppiatt et al., 2006). Furthermore, in adult and aging brain, pericyte loss can lead to brain vascular damage, including diminished capillary perfusion, impaired cerebral blood flow (CBF) response to stimulus and BBB breakdown (Bell et al., 2010).

[1]Departments of Pediatrics and Cell and Developmental Biology, University of Colorado School of Medicine, Aurora, CO 80045, USA. [2]Division of Basic Science, Fred Hutchinson Cancer Research Center, Seattle, WA 98109, USA.

*Author for correspondence (bruce.appel@ucdenver.edu)

**Received 1 March 2013; Accepted 20 October 2013**

Brain vSMCs and pericytes have been implicated in various human diseases and pathological conditions (Armulik et al., 2011; Winkler et al., 2011). For example, CADASIL (cerebral autosomal dominant arteriopathy with subcortical infarcts and leukoencephalopathy), the most common form of hereditary stroke disorder, is characterized by arteriopathy associated with the degeneration and loss of vSMCs in the brain (Salloway and Hong, 1998). Another example is intraventricular hemorrhage (IVH), which initiates in the germinal matrix (GM) and is the most common form of neonatal intracranial hemorrhage (ICH). GM is a highly vascularized brain region that has less pericyte coverage than the rest of the brain in human fetuses (Braun et al., 2007), suggesting that a low density of pericytes might account for the fragile vasculature in premature infants (Braun et al., 2007). Pericyte loss and subsequent increase of vessel permeability may also promote neurodegeneration in the aging brain (Bell et al., 2010; Sengillo et al., 2012). Despite the important implications of brain pericytes in human health, the molecular mechanisms that regulate their development, survival and distribution remain poorly understood.

During development, pericytes, derived from both neural crest and mesodermal sources (Asahina et al., 2011; Bergwerff et al., 1998; Etchevers et al., 2001; Korn et al., 2002; Que et al., 2008; Wilm et al., 2005; Yamanishi et al., 2012), expand in number and migrate to cover endothelial tubes. A combination of cell culture and mouse investigations revealed that signaling mediated by PDGF receptor β (PDGFRβ) promotes pericyte attachment to endothelial cells, migration and proliferation (Hellström et al., 1999; Lindahl et al., 1997; Tallquist et al., 2003), but how these distinct biological functions are controlled by one signaling pathway remains unknown. Another signaling mechanism implicated in pericyte development and maintenance is the Notch pathway (Domenga et al., 2004; High et al., 2007; High et al., 2008; Liu et al., 2010; Manderfield et al., 2012; Wang et al., 2012). vSMCs and pericytes express the Notch3 receptor (Domenga et al., 2004; Joutel et al., 2000; Joutel et al., 2010) and the majority of CADASIL patients have *NOTCH3* missense mutations (Joutel et al., 1996; Joutel et al., 1997). Postnatal maturation of arterial vSMCs was defective in *Notch3* knockout mice (Domenga et al., 2004), raising the possibility that Notch3 promotes mural cell differentiation. However, *in vitro* studies have produced conflicting data regarding whether Notch signaling promotes or inhibits vSMC differentiation (Doi et al., 2006; Morrow et al., 2005; Noseda et al., 2006; Proweller et al., 2005). Additionally, *Notch3* mutant mice had substantially fewer mural cells on retinal blood vessels (Liu et al., 2010), raising the possibility that Notch3 promotes mural cell specification, proliferation or survival. Consistent with this, *in vitro* studies showed that Notch signaling can promote vSMC proliferation and survival (Sakata et al., 2004; Sweeney et al., 2004; Wang et al., 2003). Notch signaling can drive PDGFRβ expression in vSMCs (Jin et al., 2008), providing a potential mechanistic link between Notch and PDGFRβ functions. Nevertheless, the precise roles that Notch signaling plays in brain pericyte development remain unclear.

Development (2014) doi:10.1242/dev.096107

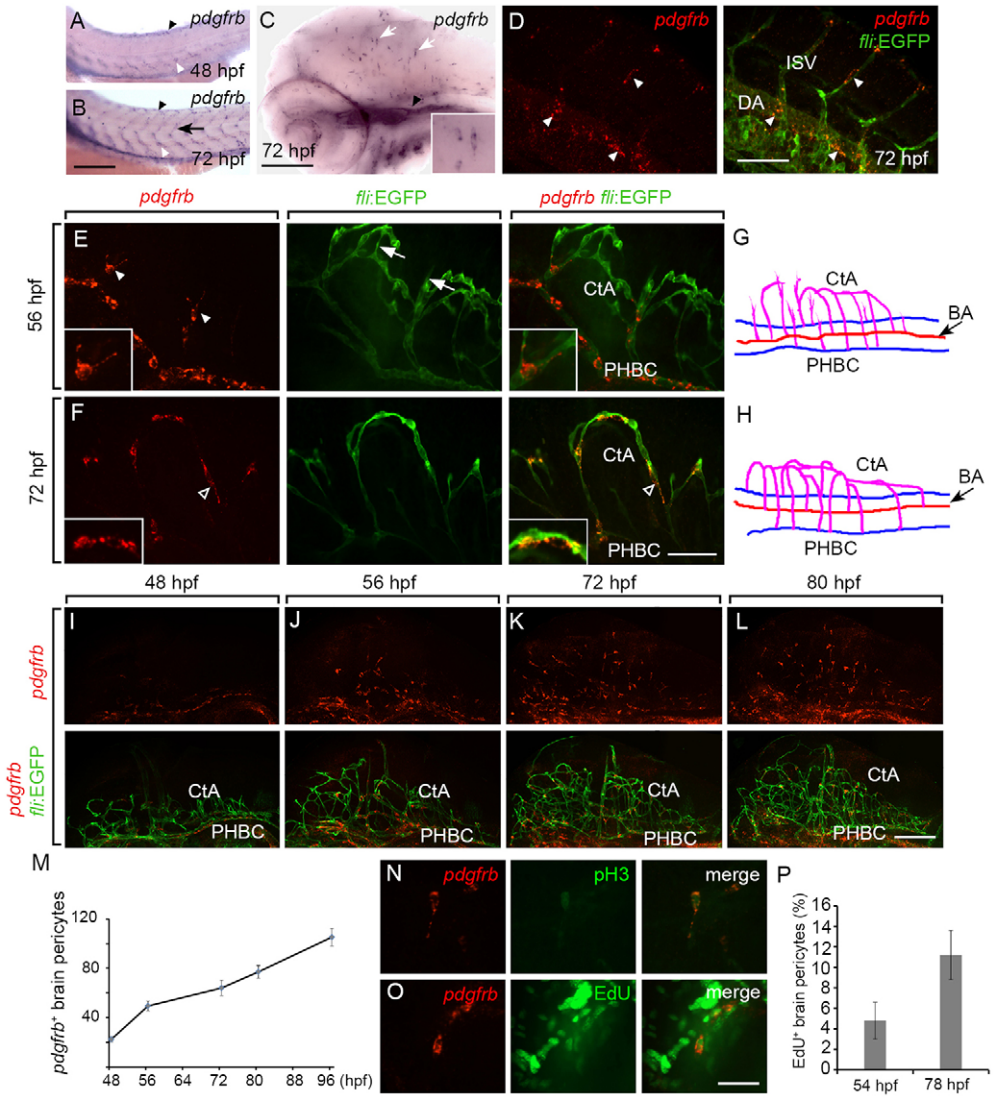


**Fig. 1. *pdgfrb* expression marks brain pericytes in zebrafish embryos and larvae.** (A,B) *pdgfrb* expression detected by ISH in trunk vasculature. Black arrowheads, DLAV; white arrowheads, DA; arrow, ISV. (C) *pdgfrb* expression in head vessels. Black arrowhead, primary head sinus; white arrows, *pdgfrb*$^{+}$ cells associated with central arteries. Inset shows a high magnification view of *pdgfrb*$^{+}$ cells in the brain. (D) Fluorescence ISH showing *pdgfrb* expression in trunk vessels (arrowheads). (E,F) Confocal sections showing *pdgfrb* expression in the hindbrain vasculature at 56 and 72 hpf, respectively. Arrowheads, Y-shape cell body of a *pdgfrb*$^{+}$ pericyte; arrows, sprouting endothelial tip cells; open arrowhead, spindle-like cell body of a *pdgfrb*$^{+}$ pericyte. Insets show a high magnification view of the *pdgfrb*$^{+}$ pericytes. (G,H) Diagrams depicting hindbrain vasculatures at 56 hpf (G) and 72 hpf (H). (I-L) Confocal projections showing *pdgfrb*$^{+}$ pericytes in the entire brain at 48, 56, 72 and 80 hpf. (M) Quantification of *pdgfrb*$^{+}$ brain pericytes at different time points during embryonic and larval development (48 hpf and 56 hpf, *n*=15 each; other time points, *n*=30 each). (N) pH3$^{+}$ *pdgfrb*$^{+}$ brain pericyte at 78 hpf. (O) EdU$^{+}$ *pdgfrb*$^{+}$ brain pericyte at 78 hpf. (P) Percentage of EdU$^{+}$ brain pericytes labeled by a 1-hour pulse at 54 hpf and 78 hpf (*n*=15 each). Error bars represent s.d. BA, basal artery; CtA, central artery; DA, dorsal aorta; ISV, intersegmental vessels; PHBC, primary hindbrain channels. Scale bars: 0.5 mm (A,B); 250 µm (C); 200 µm (D-F,I-L); 40 µm (N,O).

In this study, we set out to test the hypothesis that Notch signaling regulates pericyte coverage of brain blood vessels during development. To do so, we used zebrafish because the relatively small and simple brain vasculature facilitates quantification of pericytes and assessment of cell division and survival. We show that zebrafish pericytes express *notch3* and that *notch3* mutant zebrafish suffer brain hemorrhage and fail to form a tight BBB. Brain pericytes were initially specified in *notch3* mutant embryos but then failed to expand in number, raising the possibility that Notch3 promotes pericyte proliferation. We tested this by expressing, in a time-dependent manner, dominant-negative and constitutively active forms of Notch3 and investigating the changes in pericyte division and number. Our data provide strong evidence that Notch3 promotes expansion of brain pericyte number by promoting cell division, raising the possibility that Notch3 signaling helps determine pericyte coverage of brain blood vessels.

## RESULTS

### Zebrafish pericytes express *pdgfrb* and *notch3*

To initiate our investigation of pericyte development in zebrafish, we set out to identify molecular markers for zebrafish vSMCs and pericytes. A panel of mammalian vSMC and pericyte markers has been reported, including smooth muscle α-actin (αSMA), Rgs5, desmin, NG2 and PDGFRβ (Armulik et al., 2011). Among these, PDGFRβ appears to be the most specific and reliable, marking both vSMCs and pericytes (Armulik et al., 2011). Two zebrafish smooth muscle α-actin homologs have been reported, *acta2* and *transgelin*, and shown to be expressed in vSMCs associated with axial vasculature (Santoro et al., 2009). Brain pericytes, however, have not been previously identified in zebrafish. Therefore, we cloned additional zebrafish homologs of mammalian pericyte marker genes and performed whole-mount *in situ* RNA hybridization (ISH) experiments to examine their expression patterns during embryonic development. We found that *pdgfrb*, a *PDGFRb* homolog, and *tagln2*, another smooth muscle α-actin homolog, appeared to be expressed in the vasculature in developing embryos (Fig. 1A-C; supplementary material Fig. S1A-C). By contrast, we did not detect vascular expression of *rgs5a*, *desmin a* or *desmin b*, or the *NG2* homolog *cspg4* (supplementary material Fig. S1E-L). Intersegmental vessels (ISVs) and brain vasculature expressed *tagln2* in 48 hours post fertilization (hpf) embryos (supplementary material Fig. S1A,C). However, by 72 hpf expression decreased in the trunk (supplementary material Fig. S1B) and became difficult to detect in the brain (supplementary material Fig. S1D), limiting the usefulness

Development (2014) doi:10.1242/dev.096107

of this marker. At 24 hpf, hypochord expressed *pdgfrb* (data not shown), as previously reported (Wiens et al., 2010). At 48 hpf, *pdgfrb* expression was associated with the dorsal aorta (DA) and the dorsal longitudinal anastomotic vessel (DLAV) (Fig. 1A). At 72 hpf, *pdgfrb*$^+$ cells were distributed along ISVs, in addition to the DA and DLAV (Fig. 1B). *pdgfrb*$^+$ cells were dispersed throughout the brain, consistent with the possibility that *pdgfrb* expression marks pericytes associated with blood vessels (Fig. 1C). To determine the cell type that expressed *pdgfrb*, we performed fluorescence ISH followed by confocal microscopy. To visualize the vasculature, we used the transgenic reporter *Tg(fli1a:EGFP)* (Lawson and Weinstein, 2002), which labels vascular endothelial cells revealing all embryonic blood vessels. In the trunk, fluorescence ISH revealed that solitary perivascular cells along the ISVs expressed *pdgfrb* (Fig. 1D). In the brain, solitary *pdgfrb*$^+$ cells were distributed along brain arteries, veins and capillaries and often extended long processes along the vessels (Fig. 1E,F). Some *pdgfrb*$^+$ cells were found at capillary branch points where they extended a process along each branch, forming a Y-shaped cell (Fig. 1E, insets). These morphological features are hallmarks of pericytes (Armulik et al., 2011). Few, if any, other cells in the brain expressed *pdgfrb*, suggesting that, at this stage, *pdgfrb* expression specifically labels pericytes. In the retina, *pdgfrb*$^+$ perivascular cells were distributed along hyaloid vessels and hyaloid artery, indicative of retinal pericytes (supplementary material Fig. S1M). These expression patterns closely resemble that of mouse *Pdgfrb*, suggesting that *pdgfrb* is a reliable marker for zebrafish pericytes.

To examine pericyte development further in the zebrafish brain, we quantified the number of *pdgfrb*$^+$ cells at various developmental stages. At 48 hpf, an average of ~20 *pdgfrb*$^+$ pericytes were associated with the large arteries and veins, such as the basilar artery (BA) and primary hindbrain channels (PHBCs) (Fig. 1I,M; supplementary material Fig. S1N). By 56 hpf, the average number had increased to ~50 (Fig. 1J,M; supplementary material Fig. S1N). At this stage, a few *pdgfrb*$^+$ cells were also associated with the angiogenic sprouting front of capillaries penetrating the brain (Fig. 1J,M). Between 56 hpf and 80 hpf, the number of pericytes steadily increased as the embryos developed (Fig. 1J-M; supplementary material Fig. S1N).

The number of pericytes could increase over time by proliferation of *pdgfrb*$^+$ cells or by specification of new pericytes from *pdgfrb*$^-$ precursors. To help distinguish between these possibilities, we investigated whether *pdgfrb*$^+$ cells divide using anti-phosphohistone H3 (pH3) labeling and incorporation of the thymidine analog 5-ethynyl-2′-deoxyuridine (EdU) as M and S phase markers, respectively. At 54 hpf, occasional pH3$^+$ *pdgfrb*$^+$ pericytes could be identified (data not shown), and ~5% incorporated EdU (average 4.8±1.8%; $n$=15) (Fig. 1P), indicating that these cells were actively dividing. At 78 hpf, ~5% of *pdgfrb*$^+$ pericytes were co-labeled with pH3 (average 5.2±1.2%; $n$=12) (Fig. 1N), and ~11% incorporated EdU during a 1-hour exposure (average 11.2±2.4%; $n$=15) (Fig. 1O,P). These observations are consistent with a model in which a small population of pericyte progenitors is specified at ~48 hpf and then proliferate to expand the population.

Previous evidence from birds and rodents suggests that brain vSMCs and pericytes derive from the neural crest (Bergwerff et al., 1998; Etchevers et al., 2001; Korn et al., 2002; Yamanishi et al., 2012). To test whether zebrafish brain pericytes also have a neural crest origin, we injected embryos with previously described antisense morpholino oligonucleotides (MOs) to reduce function of *foxd3*, which interferes with neural crest formation (Stewart et al., 2006). *foxd3* MO-injected zebrafish embryos had significantly fewer

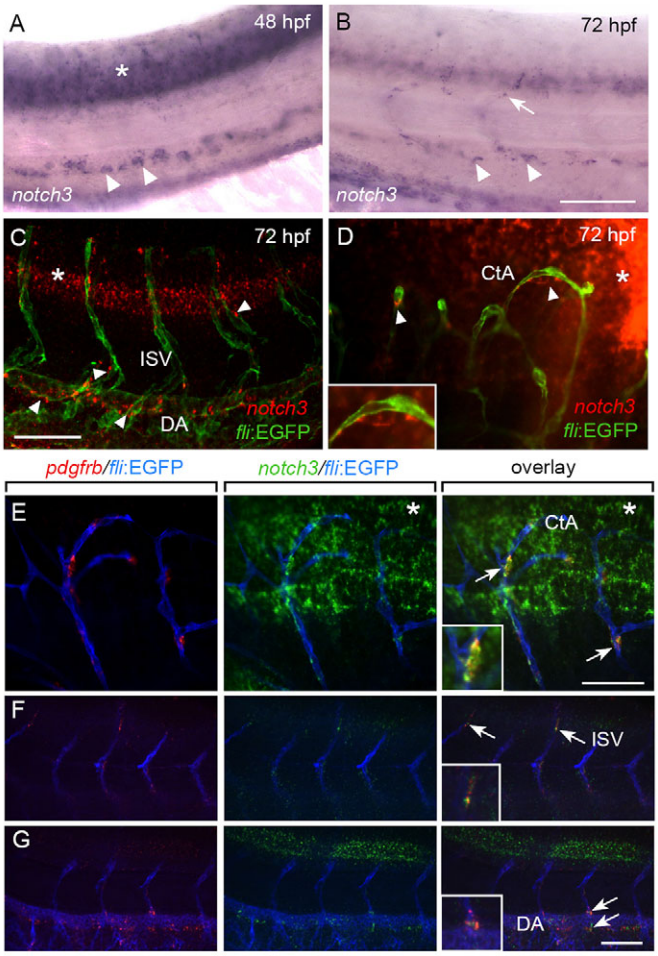


**Fig. 2. Zebrafish pericytes express *notch3*.** (A,B) *notch3* expression in the trunk vessels. Arrowheads, DA; arrow, ISVs; asterisk, neural expression. (C,D) Fluorescence ISH showing *notch3* expression in trunk (C) and brain pericytes (D). Arrowheads indicate *notch3*$^+$ pericytes and asterisk marks neural expression. Inset shows a high magnification view of a *notch3*$^+$ pericyte. (E) Double fluorescence ISH showing colocalization of *pdgfrb* and *notch3* transcripts in brain pericytes. Asterisks mark neural expression of *notch3*. (F,G) Double fluorescence ISH showing colocalization of *pdgfrb* and *notch3* transcripts in trunk vessels. (F) Confocal section showing ISV pericytes. (G) DA mural cells. Arrows indicate *pdgfrb*$^+$ *notch3*$^+$ pericytes. Insets show high magnification views of *pdgfrb* and *notch3* co-expression in pericytes. CtA, central artery; DA, dorsal aorta; ISV, intersegmental vessels. Scale bars: 200 µm.

*pdgfrb*$^+$ pericytes (average 34.8±5.9, $n$=18) in the brain than the control group (average 63.9±5.5, $n$=18) (supplementary material Fig. S1O,P), therefore supporting a neural crest origin for zebrafish brain pericytes.

To identify Notch receptors that potentially regulate mural cell development, we performed ISH to examine expression patterns of known zebrafish Notch receptor genes, including *notch1a*, *notch1b*, *notch2* and *notch3*. Of these, *notch3* showed distinct vascular expression. At 48 hpf, cells associated with the DA expressed *notch3* (Fig. 2A). By 72 hpf, *notch3* was evident along the DA and ISVs (Fig. 2B). Similar to *pdgfrb*, trunk and brain perivascular cells with mural cell-like morphology, but not endothelial cells, expressed *notch3* (Fig. 2C,D). Double ISH experiments confirmed that brain and trunk perivascular cells co-express *pdgfrb* and *notch3* transcripts (Fig. 2E-G). By contrast, fluorescence ISH did not reveal

Development (2014) doi:10.1242/dev.096107

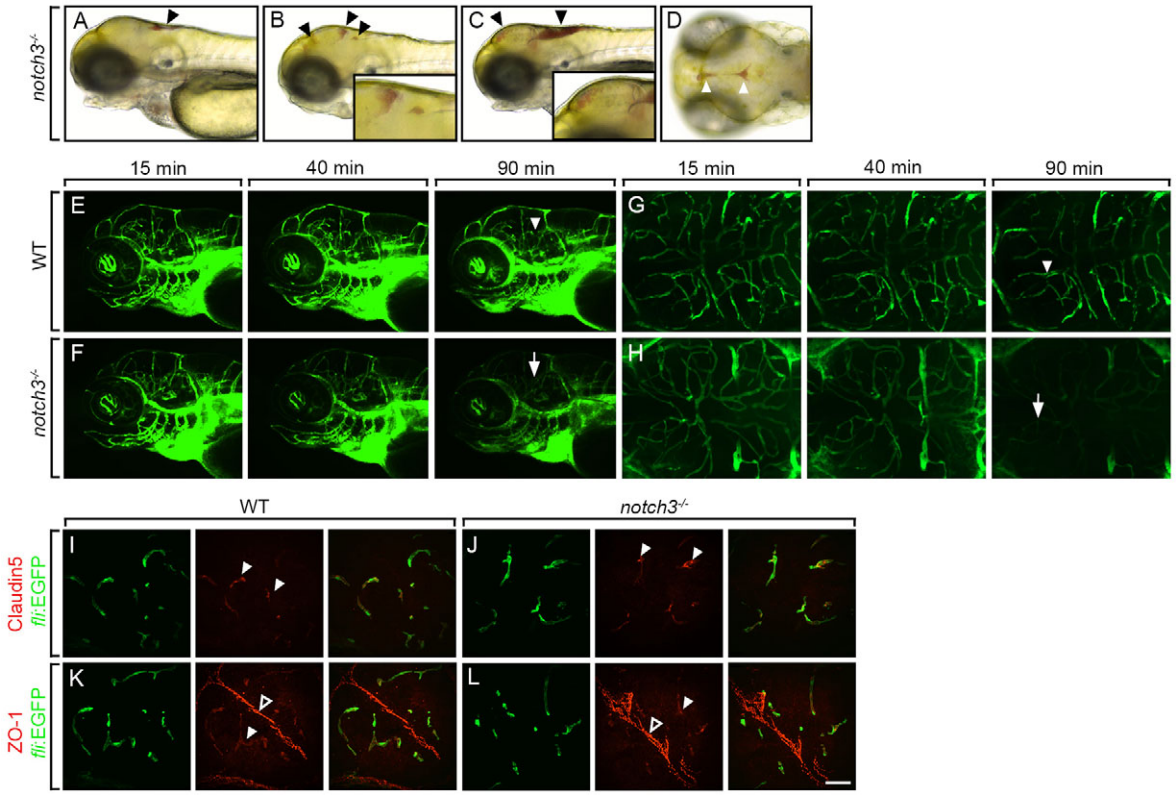


**Fig. 3. *notch3*$^{fh332}$ mutant larvae have brain hemorrhage and a defective BBB.** (A-D) Examples of brain hemorrhage in 3 dpf *notch3*$^{fh332}$ mutant larvae. (A-C) Lateral view. (D) Dorsal view. Arrowheads indicate blood pooling in the brain ventricle. Insets show high magnification view of the hemorrhage in the brain ventricle. (E-H) Representative results of BBB assay in 4 dpf wild-type (WT) and mutant larvae. (E,F) Lateral views of the brain. (G,H) Dorsal views of the midbrain and hindbrain. Mutant embryos failed to retain 2000 kD Alexa488-dextran in the brain microvessels 90 minutes after the injection. Arrowheads and arrows indicate brain vessels in the wild-type and mutant larvae, respectively. (I-L) Immunostaining of 3 dpf wild-type and mutant larvae with Claudin 5 and ZO-1 antibodies. Arrowheads indicate Claudin 5 or ZO-1 staining at the blood vessels. Open arrowheads indicate ZO-1 staining along brain ventricular wall. Scale bar: 200 µm.

perivascular expression of *notch1a*, *notch1b* or *notch2* (data not shown). These results are consistent with previous reports from mouse studies showing that mural cells, but not endothelial cells, express *Notch3* (Joutel, 2011).

### Loss of *notch3* function causes intraventricular hemorrhage and disrupts the BBB

To investigate functions of Notch3 signaling in pericyte development, we first examined embryos and larvae homozygous for a previously identified nonsense mutation of *notch3* (Alunni et al., 2013). The *notch3* $^{fh332}$ allele is predicted to generate a non-functional truncated protein lacking the entire intracellular domain and half of the EGF repeats of the extracellular domain (Alunni et al., 2013). Mutant larvae showed distinct trunk curvature at 3 days post fertilization (dpf), but otherwise appeared morphologically normal (supplementary material Fig. S2A,B). Later, a large percentage of mutant larvae developed heart edema and the majority died before 15 dpf. A small percentage of homozygous mutant animals were able to survive up to 2 months, but subsequently died before they could reach adulthood. To analyze how this mutation affects Notch activity in the animal, we crossed into the mutant background the Notch activity reporter line *Tg(Tp1bglob:hmgb1-mCherry)*, in which a nuclear mCherry fluorescent reporter is expressed under the control of an element containing 12 RBP-Jκ binding sites (Parsons et al., 2009). At 3 dpf, homozygous mutants showed significantly reduced mCherry fluorescent intensity compared with wild-type siblings (supplementary material Fig. S2C-F). We next used ISH to analyze expression of known targets of canonical Notch signaling including *her4.1*, *her2*, *hey1*, *her6* and *her9*. We found that expression of *her4.1*, *her2* and *her6* was similar between mutant and wild-type larvae at 3 dpf (supplementary material Fig. S2G,H; data not shown) and 5 dpf (data not shown). By contrast, *hey1* and *her9* were significantly reduced in 3 dpf mutant larvae (supplementary material Fig. S2I-L). These observations suggest that *hey1* and *her9* are most likely to be downstream targets of Notch3 signaling.

Strikingly, a portion of 3 dpf mutant larvae had hemorrhage within the brain but in no other tissues (Fig. 3A-D). The penetrance of the hemorrhage phenotype was variable, affecting 6.3-19.5% and 12.5-28.9% of homozygous larvae produced by matings of heterozygous carriers on AB and *Tg(fli1a:EGFP)* genetic backgrounds, respectively (supplementary material Table S1). Typically, one to four hemorrhage sites were evident in the brain, mostly located within or near the brain ventricles, characteristic of intraventricular hemorrhage (Fig. 3A-D). Expressivity of the phenotype also varied, ranging from small focal hemorrhages (Fig. 3A,B) to a broader hemorrhage across the entire intraventricular region (Fig. 3C,D). To determine whether the hemorrhagic phenotype could be exacerbated by cardiovascular stress, we raised embryos at 32°C, inducing an ~20% increase in heart rate in embryos as previously described (Barrionuevo and Burggren, 1999). This increased the hemorrhage rate to >50% in 3

Development (2014) doi:10.1242/dev.096107

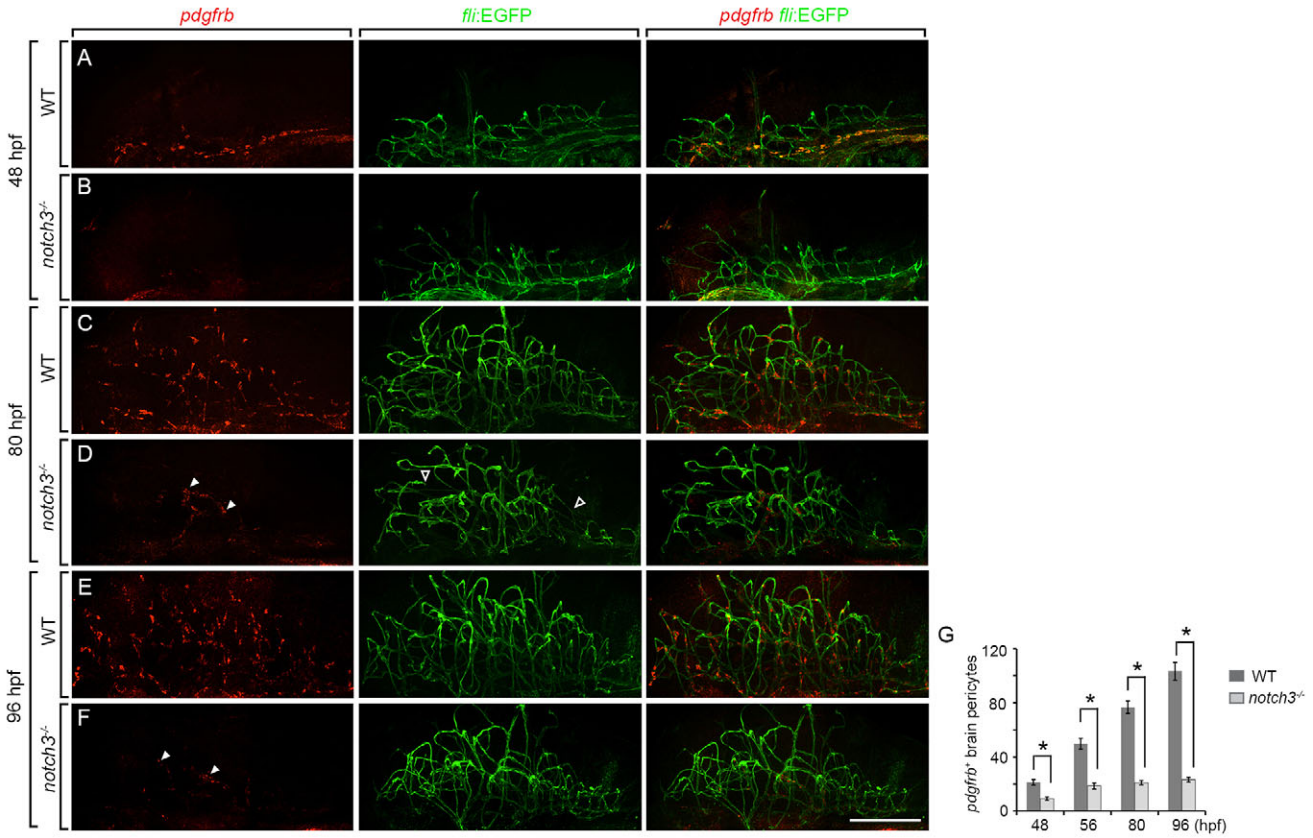


**Fig. 4. *notch3*$^{fh332}$ mutants have a deficit of pericytes.** (A-F) *pdgfrb*$^{+}$ brain pericytes in wild-type (WT) and mutant fish. Arrowheads, *pdgfrb*$^{+}$ pericytes in the mutant larvae; open arrowheads, reduced vessel branching in forebrain and hindbrain. All images show confocal projections of whole brains from lateral view with dorsal up and anterior to the left. (G) Quantification of *pdgfrb*$^{+}$ brain pericytes at different time points during embryonic and larval development in wild-type and mutant fish ($n \geq 25$ each). *$P<0.001$ by Student's two-tailed *t*-test. Scale bar: 200 µm.

dpf *notch3*$^{fh332}$ homozygous larvae on the *Tg(fli1:EGFP)* background.

One possible explanation for the brain bleeding resulting from loss of Notch3 activity is that Notch3 is required for BBB function. To test this, we injected the tracing dye Alexa Fluor 488-dextran (2000 kD) into the vasculature (Jeong et al., 2008; Xie et al., 2010) of 4 dpf wild-type larvae and similarly staged *notch3*$^{fh332}$ mutant larvae that did not show evidence of brain hemorrhage. In the wild-type larvae, the fluorescent dye was retained by the brain vasculature 90 minutes post injection (Fig. 3E,G), consistent with previous reports that a functional BBB has been established at this stage (Jeong et al., 2008; Xie et al., 2010). By contrast, the dye diffused from the brain vasculature of *notch3*$^{fh332}$ mutant larvae shortly after injection, with little fluorescence retained by the brain vessels 90 minutes after injection ($n$=10 wild-type and mutant larvae) (Fig. 3F,H). We also injected a smaller size dextran dye (10 kD FITC-dextran) and the tracing dye Evans Blue (950 Da). These dyes were also partially retained by the wild-type but not the mutant larva (supplementary material Fig. S3A-H). These data support the possibility that the brain hemorrhage of *notch3*$^{fh332}$ mutant larvae results from an abnormally formed BBB.

The hemorrhage phenotype and defective BBB could be explained by structural defects in vascular endothelial cells. To investigate this possibility, we examined expression of markers of endothelial cell differentiation. No differences in expression of *cdh5*, encoding VE-cadherin, and *cldn5b*, encoding the tight junction protein Claudin 5, transcripts (supplementary material Fig. S3I-L) or Claudin 5 and ZO-1 proteins (Fig. 3I-L) were apparent between mutant and wild-type larvae ($n$=8 wild-type and mutant larvae). Furthermore, we did not identify defects in endothelial tight junction formation by electron microscopy in either non-hemorrhagic or hemorrhagic mutant larvae ($n$=7 wild-type and mutant larvae) (supplementary material Fig. S3M-P). Together, these data indicate that Notch3 is required for brain vascular integrity, independently of endothelial cell tight junction formation.

### Notch3 function is required for pericyte development

To facilitate analysis of the vascular phenotype, we crossed the *Tg(fli1a:EGFP)* transgene into the *notch3*$^{fh332}$ mutant background. Transgene expression revealed normal vessel patterning in the trunk of mutant embryos (supplementary material Fig. S4A,B). Brain vessels showed normal patterning at 48 hpf (Fig. 4A,B), but later appeared to have reduced branching, resulting in a less elaborate vascular network at 72 hpf (Fig. 4C,D; supplementary material Fig. S4C). We next investigated pericyte development by examining *pdgfrb* expression. At 48 hpf, *notch3*$^{fh332}$ mutant embryos had significantly fewer brain *pdgfrb*$^{+}$ pericytes compared with wild type (Fig. 4A,B,G). At 72 hpf, the brain vasculature was well covered by *pdgfrb*$^{+}$ pericytes in wild-type larvae, whereas in mutant larvae only an average of ~20 *pdgfrb*$^{+}$ pericytes could be detected near the BA and PHBC, and the rest of the brain lacked *pdgfrb* expression (Fig. 4C,D,G). At 4 dpf, the number of *pdgfrb*$^{+}$ pericytes remained largely unchanged in mutant larvae, whereas their number had significantly increased in wild type (Fig. 4E-G). ISH using the

Development (2014) doi:10.1242/dev.096107

*notch3* probe also revealed a near absence of *notch3*$^{+}$ pericytes in the mutant brain (supplementary material Fig. S4D,E).

To confirm that the pericyte deficiency phenotype was caused by Notch3 loss of function, we also performed knockdown experiments using a previously described *notch3* translation-blocking MO (Leslie et al., 2007). Injection of 7 ng MO resulted in partially penetrant IVH [31.6% to 42.2% on the *Tg(fli1a:EGFP)* background] and significant reduction of *pdgfrb*$^{+}$ pericyte number compared with control, resembling the *notch3* mutant phenotype ($n$=26 each) (supplementary material Fig. S5 and Table S1), indicating that the pericyte deficit phenotype of *notch3*$^{fh332}$ mutant larvae is caused by Notch3 loss of function.

Because brain pericytes appear to derive from cranial neural crest, one possible explanation for the brain pericyte deficit in *notch3*$^{fh332}$ mutant larvae is that they are deficient for neural crest. To test this possibility, we examined expression of the pan-neural crest markers *crestin* and *sox10* by whole-mount ISH. At 24 hpf, mutant and wild-type embryos similarly expressed both genes ($n$=5 each for each gene) (supplementary material Fig. S6A-D), indicating that the brain pericyte deficit in *notch3*$^{fh332}$ mutants was not caused by impaired neural crest specification.

Previous data show that Notch signaling regulates arterial-venous differentiation. Mutation of *mind bomb*, which encodes an E3 ligase necessary for efficient Notch signaling, reduced expression of arterial markers, including *efnb2a* and *dlc*, at the dorsal aorta (Lawson et al., 2001). To determine whether the pericyte deficit might be caused by impaired arterial-venous differentiation as a result of Notch3 loss of function, we examined the expression of *ephrin B2a* and *dlc*. Notably, *notch3* $^{fh332}$ mutants expressed *efnb2a* and *dlc* in a similar pattern to wild type ($n$=8 wild-type and mutant embryos for each gene) (supplementary material Fig. S6E-H). Expression of the arterial marker *flt1* and venous marker *dab2* (Bussmann et al., 2011) were also indistinguishable between mutant and wild-type brains (supplementary material Fig S6I-L). These observations suggest that Notch3 function is dispensable for arterial-venous differentiation. Notch signaling also regulates endothelial tip cell selection in the developing vasculature whereby loss of *mind bomb* or *delta-like 4* (*dll4*) function cause an overabundance of angiogenic cells and ectopic sprouting in ISVs (Leslie et al., 2007; Siekmann and Lawson, 2007; Zygmunt et al., 2011). However, examination of *Tg(fli1a:EGFP)*;*notch3*$^{fh332}$ embryos and larvae between 2 and 3 dpf did not reveal any ectopic angiogenic sprouting (Fig. 4C-F; supplementary material Fig. S4A,B), indicating that Notch3 is not involved in determining endothelial tip cell formation.

Our data raise the possibility that the IVH and leaky BBB of *notch3* mutant larvae result from a deficit of pericytes. If so, an independent method of disrupting pericyte development should produce a similar phenotype. To test this hypothesis, we treated developing zebrafish embryos with the PDGFRβ inhibitor AG1295, a potent blocker of mural cell proliferation *in vitro* (Banai et al., 1998). At 25 μM, larvae treated with AG1295 from 32 hpf to 72 hpf or from 48 hpf to 72 hpf did not show major developmental delay, yet ISH revealed that drug-treated larvae had a significant decrease in *pdgfrb*$^{+}$ cell number in the brain ($n$≥30 for each treatment group) (supplementary material Fig. S7A-C). By 3 dpf, drug-treated larvae on the AB genetic background had a consistent intracranial hemorrhage phenotype, affecting 4.8-10.8% of treated embryos (supplementary material Fig. S7D-I and Table S1). Similar to *notch3*$^{fh332}$ mutants, the hemorrhage rate was enhanced on a *Tg(fli1a:EGFP)* background to 16.7-31% (supplementary material Table S1). The majority of hemorrhage sites were within the brain ventricles and behind the eyes (supplementary material Fig. S7E-I). Taken together, these observations support the notion that a reduced pericyte population, resulting from loss of Notch3 function, compromises the BBB and brain vascular integrity.

### Notch3 promotes brain pericyte proliferation

To test further the requirement of Notch3 signaling for promoting expansion of pericyte number, we created the transgenic line *Tg(hsp70I:N3ECD-EGFP)* to express the extracellular domain of Notch3 (N3ECD), which dominantly interferes with Notch3 function (Haruki et al., 2005; Rebay et al., 1993), fused to EGFP under control of a heat-inducible promoter (supplementary material Fig. S8A). Upon heat shock, transgenic embryos induced uniform EGFP expression (supplementary material Fig. S8B). Heat shock of *Tg(hsp70I:N3ECD-EGFP)* embryos at 30 hpf resulted in trunk curvature at 3 dpf (supplementary material Fig. S8D,E), reminiscent of *notch3*$^{fh332}$ mutant larvae. To assess how N3ECD overexpression affects Notch activity, we crossed *Tg(hsp70I:N3ECD-EGFP)* carriers to *Tg(Tp1bglob:hmgb1-mCherry)* carriers. Heat shock of *Tg(hsp70I:N3ECD-EGFP)*;*Tg(Tp1bglob:hmgb1-mCherry)* embryos at 30 hpf or 48 hpf resulted in significant reduction of mCherry expression between 3 dpf and 5 dpf (supplementary material Fig. S8F-M), resembling *notch3*$^{fh332}$ mutants. N3ECD-expressing larvae and control larvae also showed reduced levels of *hey1* and *her9* expression (supplementary material Fig. S8P-S), similar to *notch3*$^{fh332}$ mutant larvae. Therefore, N3ECD overexpression appears to reproduce Notch3 loss of function. ISH revealed that *pdgfrb*$^{+}$ pericyte number was significantly reduced in *Tg(hsp70I:N3ECD-EGFP)* larvae at 72 hpf, phenocopying *notch3*$^{fh332}$ mutant larvae (Fig. 5A,B,D). A later heat shock at 48 hpf also resulted in significant reduction in *pdgfrb*$^{+}$ pericyte number, albeit less severely (Fig. 5C,D). Similarly, a heat shock at 72 hpf resulted in significant reduction of *pdgfrb*$^{+}$ pericyte number at 96 hpf (average 80±9.9, $n$=15) compared with the control group (average 106±9.2, $n$=15). These results are consistent with the hypothesis that Notch3 positively regulates pericyte proliferation. Notably, although 48 hpf heatshock caused significant reduction in pericyte number, vascular patterning in the brain appeared largely normal compared with the control (Fig. 5A,C). Therefore, inactivation of Notch3 signaling after initial specification of pericyte progenitors appeared to abolish the expansion of these cells without causing major defects in vascular morphogenesis.

To directly test if Notch3 regulates pericyte proliferation, we examined EdU incorporation after induction of N3ECD expression. Transgenic and non-transgenic larvae were heat-shocked at 72 hpf and EdU-pulsed for 1 hour at 78 hpf. *Tg(hsp70I:N3ECD-EGFP)* larvae had significantly fewer pericytes than the control group and the percentage of EdU$^{+}$ brain pericytes (number of *pdgfrb*$^{+}$EdU$^{+}$ brain pericytes/total number of *pdgfrb*$^{+}$ brain pericytes) was significantly decreased (Fig. 5E).

Next, to determine whether Notch3 signaling is sufficient for promoting brain pericyte proliferation, we overexpressed the Notch3 intracellular domain (Notch3ICD, or N3ICD) as a constitutively activated form of Notch3. To do this, we generated the transgenic line *Tg(hsp70I:N3ICD-EGFP)*, in which EGFP-tagged N3ICD is expressed under the control of the heat shock promoter (supplementary material Fig. S8A). Transgenic embryos induced uniform EGFP signal after heat shock (supplementary material Fig. S8C). In the majority of embryos, the EGFP fluorescence gradually faded away after ~10 hours, probably owing to protein degradation mediated by the PEST domain at the C-terminus of N3ICD. This transgenic line therefore allows heat shock-induced, transient activation of Notch3 signaling in an ~10-hour

Development (2014) doi:10.1242/dev.096107

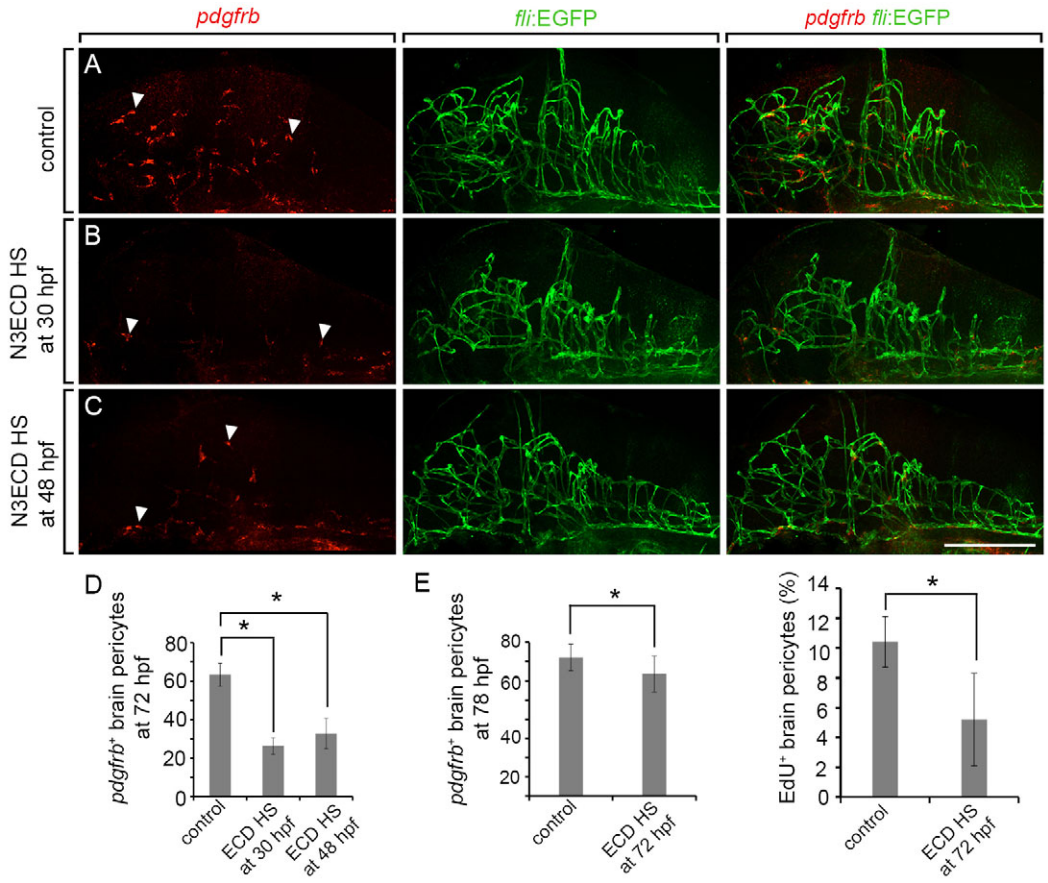


**Fig. 5. Notch3 is required for brain pericyte proliferation.** (A-C) N3ECD-GFP overexpression results in fewer *pdgfrb*$^{+}$ brain pericytes at 72 hpf. (A) Non-transgenic control fish. (B,C) *Tg(hsp70l:N3ECD-GFP)* larvae heat-shocked at 30 hpf and 48 hpf. Arrowheads, *pdgfrb*$^{+}$ brain pericytes. (D) Quantification of *pdgfrb*$^{+}$ brain pericytes in control and *Tg(hsp70l:N3ECD-GFP)* larvae at 72 hpf ($n$≥31 each). (E) Quantification of brain pericytes and percentage of EdU$^{+}$ pericytes in control and *Tg(hsp70l:N3ECD-GFP)* larvae heat-shocked at 72 hpf and EdU pulsed at 78 hpf ($n$=42 each). Error bars represent s.d. *$P$<0.001 by Student's two-tailed $t$-test. Scale bar: 200 µm.

time window. Heat-shocked *Tg(hsp70I:N3ECD-EGFP)*; *Tg(Tp1bglob:hmgb1-mCherry)* embryos showed a robust increase in mCherry fluorescence intensity compared with control (supplementary material Fig. S8N,O), confirming that N3ICD overexpression is capable of triggering RBP-Jκ-mediated transcriptional activation. We then performed heat shock at different stages and examined pericyte development at 72 hpf. After an early heat shock at 30 hpf, we did not observe a significant change in *pdgfrb* expression at 72 hpf, suggesting that Notch3 overexpression alone is not sufficient to induce ectopic pericyte specification (supplementary material Fig. S9A,B). By contrast, heat shock at 48 hpf induced a significant increase in the number of *pdgfrb*$^{+}$ pericytes (Fig. 6A,B,E), supporting the hypothesis that Notch3 signaling expands the pericyte population once they are specified. To test if Notch3 overexpression promotes pericyte division, we examined EdU incorporation after induction of N3ICD expression. Larvae were heat-shocked at 72 hpf and subjected to an EdU pulse of 1 hour at 78 hpf. We found that the number of *pdgfrb*$^{+}$ pericytes and the percentage of *pdgfrb*$^{+}$ pericytes that incorporated EdU were significantly increased in *Tg(hsp70I:N3ICD-EGFP)* larvae compared with controls (Fig. 6F). Therefore, Notch3 appears to be sufficient for promoting brain pericyte proliferation.

Pdgfb/Pdgfrβ signaling can promote pericyte proliferation (Olson and Soriano, 2011) and in cell culture constitutively active Notch3 can elevate *Pdgfrb* expression (Jin et al., 2008), raising the possibility that Notch3 regulates pericyte number and vascular integrity, at least in part, by regulating *Pdgfrb* transcription. We performed two experiments to investigate whether Notch3 and Pdgfrβ function in a common pathway to regulate pericyte development *in vivo*. First, we reasoned that if Notch3 regulates vascular integrity via Pdgfrβ, then a low dose of the AG1295 inhibitor should enhance the *notch3* loss-of-function phenotype. Indeed, *notch3*$^{fh332}$ homozygous mutants showed a more penetrant hemorrhage phenotype when treated with a low dose of AG1295 that, by itself, did not alter pericyte number in wild-type larvae ($n$=5; supplementary material Fig. S7J). Second, if Notch3 works through Pdgfrβ, then the increase in pericyte number resulting from expression of constitutively active Notch3 should require Pdgfrβ function. To test this, we treated heat-shocked *Tg(hsp70I:N3ICD-EGFP)* larvae with 25 µM AG1295. This resulted in reduction in brain pericyte number to a similar extent as in AG1295-treated control larvae (Fig. 6G).

Finally, we tested whether Notch3 overexpression could rescue Notch3 loss of function. First, we transiently expressed N3ICD by injecting the *hsp70I:Notch3ICD-EGFP* construct into *notch3*$^{fh332}$ mutant embryos and heat shocking at 48 hpf. This partially rescued the pericyte deficiency phenotype in about half of the injected mutant embryos ($n$=11/23) (supplementary material Fig. S9C,D). To confirm this observation, we then crossed the *hsp70I:Notch3ICD-EGFP* transgene into the *notch3*$^{fh332}$ mutant background. Heat shock

Development (2014) doi:10.1242/dev.096107

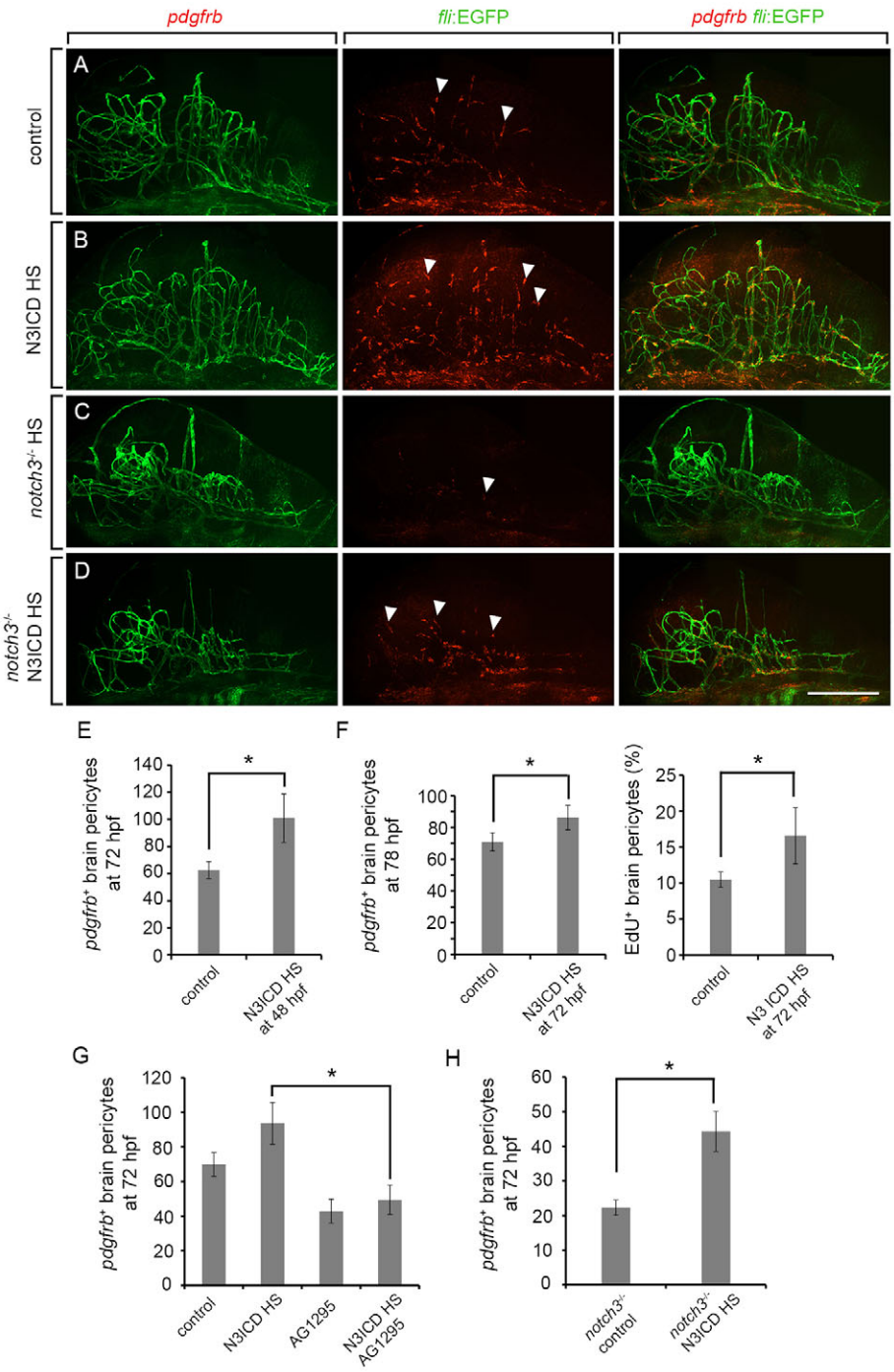


**Fig. 6. Notch3 is sufficient to promote brain pericyte proliferation.** (A,B) N3ICD-EGFP overexpression increased the number of *pdgfrb*$^{+}$ brain pericytes at 72 hpf. (A) Non-transgenic control larvae. (B) *Tg(hsp70l:N3ICD-EGFP)* larva heat-shocked (HS) at 48 hpf. (C,D) N3ICD overexpression rescued the brain pericyte deficit phenotype in *notch3*$^{fh332}$ mutant larvae at 72 hpf. (C) *notch3*$^{fh332}$ homozygous larvae heat-shocked at 48 hpf. (D) *notch3*$^{fh332}$ homozygous larvae carrying the *Tg(hsp70l:N3ICD-EGFP)* transgene and heat shocked at 48 hpf. Arrowheads, *pdgfrb*$^{+}$ brain pericytes. (E) Quantification of *pdgfrb*$^{+}$ brain pericytes in control and N3ICD fish at 72 hpf ($n$=30 each). (F) Quantification of brain pericytes and percentage of EdU$^{+}$ pericytes in control and N3ICD fish heat-shocked at 72 hpf and EdU pulsed at 78 hpf ($n$=25 each). (G) Quantification of brain pericytes at 72 hpf in control larvae, N3ICD larvae heat-shocked at 48 hpf, control larvae treated with 25 µM AG1295, and N3ICD larvae heat-shocked at 48 hpf immediately followed by AG1295 treatment ($n$≥20 each). (H) Quantification of brain pericytes at 72 hpf in *notch3*$^{fh332}$ larvae heat shocked at 48 hpf (control group) and *notch3*$^{fh332}$;*Tg(hsp70l: N3ICD-EGFP)* larvae heat shocked at 48 hpf. Error bars represent s.d. *$P$<0.001 by Student's two-tailed $t$-test. Scale bar: 200 µm.

at 48 hpf significantly rescued the pericyte deficiency phenotype in all homozygous mutant embryos ($n$=15) (Fig. 6C,D,H). Notably, despite the significant rescue of the pericyte phenotype, the vascular branching defect was not rescued by N3ICD expression (Fig. 6C,D). Heat shock of *notch3*$^{fh332}$;*Tg(hsp70l:N3ICD-EGFP)* embryos at 30 hpf did not rescue the pericyte deficiency ($n$=14; data not shown), consistent with our previous observation that heat shock of *Tg(hsp70l:N3ICD-EGFP)* embryos at 30 hpf did not expand the pericyte population. Overexpression of Notch3ICD in endothelial cells by injection of the expression construct *fli1:myc-Notch3ICD* (Lawson et al., 2001) failed to rescue the phenotype ($n$=15) (supplementary material Fig. S9E,F). Therefore, endothelial cell expression of Notch3ICD is not sufficient to promote pericyte proliferation. Taken together with our data showing pericyte-specific expression of *notch3*, these results provide evidence that Notch3 function is required within pericytes to promote their proliferation. We conclude that Notch3 signaling within pericytes drives expansion of the population through proliferation, thereby providing an essential role in establishing brain vascular integrity.

## DISCUSSION

Consistent with the recently documented requirement of pericytes in BBB formation and function, *notch3*$^{fh332}$ mutant larvae frequently had brain hemorrhage, and even those without obvious blood pooling had a leaky BBB. We found no evidence of endothelial cell abnormalities by electron microscopy, indicating that, at these early

Development (2014) doi:10.1242/dev.096107

stages of development, hemorrhage probably resulted from impaired BBB function rather than from a failure of endothelial cell differentiation. Therefore, the small number of pericytes that develop in *notch3*$^{fh332}$ mutants is not sufficient to direct BBB formation, indicating that Notch3 function is part of a mechanism to promote adequate pericyte coverage of brain vessels. Notably, a recent study using independently identified *notch3* hypomorphic alleles suggested that reduced Notch3 signaling compromised vascular tone and vascular integrity in the fins of adult zebrafish (Zaucker et al., 2013). Mural cells could not be unambiguously identified in the fin vasculature of *notch3* mutants, supporting our own results.

Previous evidence suggested that Notch3 signaling promotes *Pdgfrb* expression. *Pdgfrb* expression was reduced by 40% in vSMCs of tail lateral arteries in newborn *Notch3*$^{lacZ/lacZ}$ mutant mice and in cell culture constitutively active Notch3 increased *Pdgfrb* transcript and protein levels (Jin et al., 2008). Our observations seem to corroborate these findings. In *notch3*$^{fh332}$ mutant and heat-shocked *Tg(hsp70I:N3ECD-EGFP)* larvae, there appeared to be a modest but noticeable reduction of *pdgfrb* transcript level in individual pericytes. Conversely, N3ICD expression appeared to increase *pdgfrb* transcript levels in individual pericytes. Furthermore, use of a pharmacological inhibitor showed that reducing Pdgfrβ enhanced the brain hemorrhage phenotype of *notch3* mutant larvae and that N3ICD-driven pericyte proliferation requires Pdgfrβ function. Because *pdgfrb* expression level appears to be an intrinsic determinant of pericyte proliferation rate (Tallquist et al., 2003), these data are consistent with a model in which a Notch3-Pdgfrβ hierarchy regulates pericyte proliferation.

Other important roles of Notch signaling in vascular development have been documented, including regulation of tip cell formation and arterial-venous differentiation (Hellström et al., 2007; Larrivée et al., 2012; Lawson et al., 2001; Lawson et al., 2002; Leslie et al., 2007). *notch3*$^{fh332}$ mutant larvae, however, showed no sign of ectopic vessel sprouting or deficient arterial differentiation as assessed by arterial marker expression. Therefore, Notch3 signaling is most likely to be dispensable for tip cell selection and arterial-venous differentiation. Conversely, *notch3*$^{fh332}$ mutant larvae had reduced brain vascular branching at 3 dpf. It remains to be determined whether this defect reflects an endothelial cell-autonomous role of Notch3 in brain vascular patterning. Nevertheless, several lines of evidence argue that the pericyte deficit of *notch3*$^{fh332}$ mutants is not secondary to reduced vascular morphogenesis. First, the pericyte deficit of *notch3*$^{fh332}$ mutant embryos was evident starting from 48 hpf, preceding the appearance of the patterning defect in the brain. Second, induction of N3ECD expression at 48 hpf resulted in reduced pericyte number at 72 hpf without significantly altering vascular patterning in the brain. Third, N3ICD induction at 48 hpf in *notch3*$^{fh332}$ mutant embryos significantly rescued the pericyte deficit phenotype, but failed to rescue the vascular patterning phenotype. Fourth, endothelial expression of N3ICD failed to rescue the pericyte deficit phenotype in *notch3*$^{fh332}$ mutants. These data are consistent with a cell-autonomous role of Notch3 in pericyte development. Indeed, existing evidence suggests that the reduced vessel branching could actually be caused by the pericyte deficit: there was a mild but measurable decrease of the number of vessel branch points in the brain of *Pdgfrb* knockout mice (Hellström et al., 2001). Additionally, a hypomorphic allele of *Pdgfrb* produced significantly fewer vessel branch points in mouse retina (Jadeja et al., 2013).

In mice, Notch signaling has been shown to cooperate with Smad4 to promote N-cadherin expression in brain endothelial cells. Brain endothelial cell-specific inactivation of Notch signaling caused impaired endothelial-pericyte adhesion, causing BBB breakdown and perinatal IVH (Li et al., 2011). This process is likely to involve Notch1 and Notch4, two Notch receptors that are expressed in endothelial cells dependent on Smad4 function (Li et al., 2011). These data, along with the results of our study, indicate that distinct Notch signaling pathways in brain pericytes and endothelial cells (Notch3 and Notch1/Notch4, respectively) work together to ensure the proper establishment of brain vascular integrity by promoting brain pericyte expansion as well as pericyte attachment to the endothelium.

Our work could also provide new insights into CADASIL pathology. The vSMC degeneration associated with CADASIL might result from abnormal signaling conferred by particular dominant missense *NOTCH3* mutations (Joutel, 2011). Our data provide strong evidence that Notch3 promotes expansion of pericyte number, perhaps by positively regulating *pdgfrb* expression. Conceivably, NOTCH3 also maintains pericyte number in the adult brain by promoting *PDGFRB* expression and replacement of pericytes lost during aging. Indeed, in mice, haploinsufficiency of *Pdgfrb* resulted in an age-dependent progressive loss of brain pericytes (Bell et al., 2010). Therefore, a reduction in the rate of replenishment of pericytes resulting from abnormal NOTCH3 signaling might contribute to the vascular defects characteristic of CADASIL.

## MATERIALS AND METHODS

### Zebrafish husbandry

The University of Colorado Anschutz Medical Campus Institutional Animal Care and Use Committee approved all zebrafish studies. Embryos were produced by pair matings and raised at 28.5°C in egg water or embryo medium and staged according to hpf or dpf. Strains in addition to new transgenic lines described below included AB, *Tg(fli1a:EGFP)* (Lawson and Weinstein, 2002), *Tg(Tp1bglob:hmgb1-mCherry)* (Parsons et al., 2009) and *notch3*$^{fh332}$ (Alunni et al., 2013).

### Generation of transgenic zebrafish

Sequences encoding N3ECD (amino acids 1-1665) and N3ICD (amino acids 1659-2468) were amplified from wild-type cDNA using the following primers: N3ECD forward, 5′-ATGGGGAATTACAGCCTTTGGAT-3′; N3ECD reverse, 5′-GGCAATCAACATGCCAACCATC-3′; N3ICD forward, 5′-ATGGTTGGCATGTTGATTGC-3′; N3ICD reverse, 5′-AGCAAACACCTGCATCTTCC-3′. Products were cloned followed by Gateway recombination to generate *hsp70I:N3ECD-EGFP* and *hsp70I:N3ICD-EGFP* using the Tol2 kit (Kwan et al., 2007). Microinjected embryos were screened and those with EGFP$^{+}$ hearts were raised. These were mated with AB fish and progeny were screened for heart EGFP expression. EGFP$^{+}$ embryos were raised to establish transgenic lines. Multiple alleles were identified for each transgenic line, and those with stronger transgene expression were designated *Tg(hsp70I:N3ECD-EGFP)*$^{co15}$ and *Tg(hsp70I:N3ICD-EGFP)*$^{co17}$.

### Whole-mount ISH

Whole-mount ISH was performed as described (Thisse and Thisse, 2008). *pdgfrb*, *tagln2*, *cspg4*, *rgs5a*, *desmin a*, *desmin b* and *notch3* sequences (GenBank accession numbers HM439112, NM_201676, XM_001923422, NM_199962, NM_130963, NM_001077452 and AF152001, respectively) were amplified from cDNA and cloned into pJC-53.2 (Collins et al., 2010). Anti-sense probes were synthesized from PCR products amplified from corresponding cDNA constructs with T7 primers. Fluorescence ISH was performed as described (Lauter et al., 2011). Fluorescent ISH samples were imaged using a microscope equipped with a PerkinElmer UltraVIEW VoX confocal system and Volocity software. Image brightness and contrast were adjusted in Volocity or ImageJ. For comparison purposes, the same adjustment was applied to all images. For quantification of brain pericytes,

*pdgfrb*$^{+}$ cells were counted in confocal *z*-stacks of whole embryonic or larval brains. For quantification of brain vessel branching, vessel branch points were counted in confocal *z*-stacks of whole larval brains.

### Immunohistochemistry and EdU labeling

Whole-mount immunohistochemistry was performed after ISH using rabbit anti-phospho-Histone-H3 (1:1000, 06570, Upstate Biotechnology) and rabbit anti-GFP (1:200, A11122, Invitrogen) antibodies. ZO-1 and Claudin 5 antibody staining were performed on 20 µm frozen sections using mouse anti-Claudin 5 (1:25, 18-7364, Invitrogen) and rabbit anti-ZO-1 (1:25, 33-9100, Invitrogen). For EdU labeling, embryos were manually dechorionated and incubated with 10 mM EdU in 10% DMSO in E3 medium for 1 hour. The embryos were then fixed using 4% paraformaldehyde in PBST (0.1% Tween) and processed for ISH. EdU detection was performed using the Click-iT EdU Imaging Kit (Invitrogen) by incubating in EdU detection cocktail for 1.5 hours.

### Transmission electron microscopy

Embryos were fixed at 4 dpf in 2% glutaraldehyde in 0.1 M sodium cacodylate buffer (pH 7.4) overnight at 4°C. Embryos were washed, postfixed with 1% osmium tetraoxide, dehydrated and embedded. Sections (50-70 nm) were cut and stained with 3% uranyl acetate and Reynolds' lead citrate.

### MO injection

MOs targeting *notch3* and *foxd3* were obtained from Gene Tools. For *notch3*, we injected 7 ng of ATG-targeting morpholino: 5′-ATATCCAAAGGCTGTAATTCCCCAT-3′ (Leslie et al., 2007). For *foxd3* knockdown, we co-injected 3.5 ng each of *foxd3*-MO$^{5UTR}$: 5′-CACCGCGCACTTTGCTGCTGGAGCA-3′, and *foxd3*-MO$^{AUG}$: 5′-CACTGGTGCCTCCAGACAGGGTCAT-3′ as described previously (Montero-Balaguer et al., 2006).

### BBB assay

For the BBB assay, 2000 kD Alexa-488 dextran (2.5 mg/ml in PBS, FD2000S, Sigma), 10 kD FITC-dextran (2.5 mg/ml in PBS, FD10S, Sigma) and Evans Blue (2% in PBS, 15110805, MP Biomedicals) were injected into the hearts of 4 dpf larvae as described (Jeong et al., 2008).

### Drug treatment

For imaging brain hemorrhage, embryos were treated with 0.001% 1-phenyl-2-thiourea (PTU) at 22 hpf to prevent pigmentation. For PDGF receptor inhibitor assays, PDGF receptor tyrosine kinase inhibitor AG1295 (Millipore) was reconstituted in DMSO to make a 1 mM stock. Embryos were treated with 1% DMSO alone or with 25 µM or 10 µM AG1295 with 1% DMSO in E3 media.

### Quantitative and statistical methods

Quantifications were performed by collecting confocal *z*-stacks of entire brains and counting pericytes from maximally projected images. *z* images were examined to distinguish between individual pericytes. Data were evaluated using Student's two-tailed *t*-test.

#### Acknowledgements

We thank Julie Siegenthaler for valuable discussions and comments on the manuscript; Nathan Lawson for the *fli1:myc-Notch3ICD* construct; James Collins for the pJC-53.2 vector; and Dorothy Dill for electron microscopy help.

#### Competing interests

The authors declare no competing financial interests.

#### Author contributions

Y.W. performed all the experiments and produced the data. Y.W. and B.A. conceived the project, interpreted results and wrote the manuscript. L.P. and C.B.M. provided the *notch3*$^{fh332}$ allele.

#### Funding

This work was supported by a gift from the Gates Frontiers Fund. The University of Colorado Anschutz Medical Campus Zebrafish Core Facility is supported by a National Institutes of Health (NIH) grant [P30 NS048154]. The *notch3*$^{fh332}$ mutant was identified by TILLING with the support of an NIH grant [RO1 HG002995 to C.B.M.]. Deposited in PMC for release after 12 months.

#### Supplementary material

Supplementary material available online at
http://dev.biologists.org/lookup/suppl/doi:10.1242/dev.096107/-/DC1

#### References

**Alunni, A., Krecsmarik, M., Bosco, A., Galant, S., Pan, L., Moens, C. B. and Bally-Cuif, L.** (2013). Notch3 signaling gates cell cycle entry and limits neural stem cell amplification in the adult pallium. *Development* **140**, 3335-3347.

**Armulik, A., Genové, G., Mäe, M., Nisancioglu, M. H., Wallgard, E., Niaudet, C., He, L., Norlin, J., Lindblom, P., Strittmatter, K. et al.** (2010). Pericytes regulate the blood-brain barrier. *Nature* **468**, 557-561.

**Armulik, A., Genové, G. and Betsholtz, C.** (2011). Pericytes: developmental, physiological, and pathological perspectives, problems, and promises. *Dev. Cell* **21**, 193-215.

**Asahina, K., Zhou, B., Pu, W. T. and Tsukamoto, H.** (2011). Septum transversum-derived mesothelium gives rise to hepatic stellate cells and perivascular mesenchymal cells in developing mouse liver. *Hepatology* **53**, 983-995.

**Banai, S., Wolf, Y., Golomb, G., Pearle, A., Waltenberger, J., Fishbein, I., Schneider, A., Gazit, A., Perez, L., Huber, R. et al.** (1998). PDGF-receptor tyrosine kinase blocker AG1295 selectively attenuates smooth muscle cell growth in vitro and reduces neointimal formation after balloon angioplasty in swine. *Circulation* **97**, 1960-1969.

**Barrionuevo, W. R. and Burggren, W. W.** (1999). O2 consumption and heart rate in developing zebrafish (Danio rerio): influence of temperature and ambient O2 O 2 consumption and heart rate in developing zebrafish (Danio rerio): influence of temperature and ambient O 2. *Am. J. Physiol.* **276**, R505-R513.

**Bell, R. D., Winkler, E. A., Sagare, A. P., Singh, I., LaRue, B., Deane, R. and Zlokovic, B. V.** (2010). Pericytes control key neurovascular functions and neuronal phenotype in the adult brain and during brain aging. *Neuron* **68**, 409-427.

**Bergwerff, M., Verberne, M. E., DeRuiter, M. C., Poelmann, R. E. and Gittenberger-de Groot, A. C.** (1998). Neural crest cell contribution to the developing circulatory system: implications for vascular morphology? *Circ. Res.* **82**, 221-231.

**Braun, A., Xu, H., Hu, F., Kocherlakota, P., Siegel, D., Chander, P., Ungvari, Z., Csiszar, A., Nedergaard, M. and Ballabh, P.** (2007). Paucity of pericytes in germinal matrix vasculature of premature infants. *Neuroscience* **27**, 12012-12024.

**Bussmann, J., Wolfe, S. A. and Siekmann, A. F.** (2011). Arterial-venous network formation during brain vascularization involves hemodynamic regulation of chemokine signaling. *Development* **138**, 1717-1726.

**Collins, J. J., III, Hou, X., Romanova, E. V., Lambrus, B. G., Miller, C. M., Saberi, A., Sweedler, J. V. and Newmark, P. A.** (2010). Genome-wide analyses reveal a role for peptide hormones in planarian germline development. *PLoS Biol.* **8**, e1000509.

**Daneman, R., Zhou, L., Kebede, A. A. and Barres, B. A.** (2010). Pericytes are required for blood-brain barrier integrity during embryogenesis. *Nature* **468**, 562-566.

**Doi, H., Iso, T., Sato, H., Yamazaki, M., Matsui, H., Tanaka, T., Manabe, I., Arai, M., Nagai, R. and Kurabayashi, M.** (2006). Jagged1-selective notch signaling induces smooth muscle differentiation via a RBP-Jkappa-dependent pathway. *J. Biol. Chem.* **281**, 28555-28564.

**Domenga, V., Fardoux, P., Lacombe, P., Monet, M., Maciazek, J., Krebs, L. T., Klonjkowski, B., Berrou, E., Mericskay, M., Li, Z. et al.** (2004). Notch3 is required for arterial identity and maturation of vascular smooth muscle cells. *Genes Dev.* **18**, 2730-2735.

**Etchevers, H. C., Vincent, C., Le Douarin, N. M. and Couly, G. F.** (2001). The cephalic neural crest provides pericytes and smooth muscle cells to all blood vessels of the face and forebrain. *Development* **128**, 1059-1068.

**Haruki, N., Kawaguchi, K. S., Eichenberger, S., Massion, P. P., Olson, S., Gonzalez, A., Carbone, D. P. and Dang, T. P.** (2005). Dominant-negative Notch3 receptor inhibits mitogen-activated protein kinase pathway and the growth of human lung cancers. *Cancer Res.* **65**, 3555-3561.

**Hellström, M., Kalén, M., Lindahl, P., Abramsson, A. and Betsholtz, C.** (1999). Role of PDGF-B and PDGFR-beta in recruitment of vascular smooth muscle cells and pericytes during embryonic blood vessel formation in the mouse. *Development* **126**, 3047-3055.

**Hellström, M., Gerhardt, H., Kalén, M., Li, X., Eriksson, U., Wolburg, H. and Betsholtz, C.** (2001). Lack of pericytes leads to endothelial hyperplasia and abnormal vascular morphogenesis. *J. Cell Biol.* **153**, 543-554.

**Hellström, M., Phng, L.-K., Hofmann, J. J., Wallgard, E., Coultas, L., Lindblom, P., Alva, J., Nilsson, A.-K., Karlsson, L., Gaiano, N. et al.** (2007). Dll4 signalling through Notch1 regulates formation of tip cells during angiogenesis. *Nature* **445**, 776-780.

**High, F. A., Zhang, M., Proweller, A., Tu, L., Parmacek, M. S., Pear, W. S. and Epstein, J. A.** (2007). An essential role for Notch in neural crest during cardiovascular development and smooth muscle differentiation. *J. Clin. Invest.* **117**, 353-363.

**High, F. A., Lu, M. M., Pear, W. S., Loomes, K. M., Kaestner, K. H. and Epstein, J. A.** (2008). Endothelial expression of the Notch ligand Jagged1 is required for vascular smooth muscle development. *Proc. Natl. Acad. Sci. USA* **105**, 1955-1959.

**Jadeja, S., Mort, R. L., Keighren, M., Hart, A. W., Joynson, R., Wells, S., Potter, P. K. and Jackson, I. J.** (2013). A CNS-specific hypomorphic Pdgfr-beta mutant model of diabetic retinopathy. *Invest. Ophthalmol. Vis. Sci.* **54**, 3569-3578.

**Jeong, J.-Y., Kwon, H.-B., Ahn, J.-C., Kang, D., Kwon, S.-H., Park, J. A. and Kim, K.-W.** (2008). Functional and developmental analysis of the blood-brain barrier in zebrafish. *Brain Res. Bull.* **75**, 619-628.

**Jin, S., Hansson, E. M., Tikka, S., Lanner, F., Sahlgren, C., Farnebo, F., Baumann, M., Kalimo, H. and Lendahl, U.** (2008). Notch signaling regulates platelet-derived growth factor receptor-beta expression in vascular smooth muscle cells. *Circ. Res.* **102**, 1483-1491.

**Joutel, A.** (2011). Pathogenesis of CADASIL: transgenic and knock-out mice to probe function and dysfunction of the mutated gene, Notch3, in the cerebrovasculature. *BioEssays* **33**, 73-80.

**Joutel, A., Corpechot, C., Ducros, A., Vahedi, K., Chabriat, H., Mouton, P., Alamowitch, S., Domenga, V., Cecilion, M., Marechal, E., et al.** (1996). Notch3 mutations in CADASIL, a hereditary adult-onset condition causing stroke and dementia. *Nature* **383**, 707-710.

**Joutel, A., Vahedi, K., Corpechot, C., Troesch, A., Chabriat, H., Vayssière, C., Cruaud, C., Maciazek, J., Weissenbach, J., Bousser, M. G. et al.** (1997). Strong clustering and stereotyped nature of Notch3 mutations in CADASIL patients. *Lancet* **350**, 1511-1515.

**Joutel, A., Andreux, F., Gaulis, S., Domenga, V., Cecillon, M., Battail, N., Piga, N., Chapon, F., Godfrain, C. and Tournier-Lasserve, E.** (2000). The ectodomain of the Notch3 receptor accumulates within the cerebrovasculature of CADASIL patients. *J. Clin. Invest.* **105**, 597-605.

**Joutel, A., Monet-leprêtre, M., Gosele, C., Baron-menguy, C., Hammes, A., Schmidt, S., Lemaire-carrette, B., Domenga, V., Schedl, A., Lacombe, P., et al.** (2010). Cerebrovascular dysfunction and microcirculation rarefaction precede white matter lesions in a mouse genetic model of cerebral ischemic small vessel disease. *J. Clin. Invest.* **120**, 433-445.

**Korn, J., Christ, B. and Kurz, H.** (2002). Neuroectodermal origin of brain pericytes and vascular smooth muscle cells. *J. Comp. Neurol.* **88**, 78-88.

**Kwan, K. M., Fujimoto, E., Grabher, C., Mangum, B. D., Hardy, M. E., Campbell, D. S., Parant, J. M., Yost, H. J., Kanki, J. P. and Chien, C.-B.** (2007). The Tol2kit: a multisite gateway-based construction kit for Tol2 transposon transgenesis constructs. *Dev. Dyn.* **236**, 3088-3099.

**Larrivée, B., Prahst, C., Gordon, E., del Toro, R., Mathivet, T., Duarte, A., Simons, M. and Eichmann, A.** (2012). ALK1 signaling inhibits angiogenesis by cooperating with the Notch pathway. *Dev. Cell* **22**, 489-500.

**Lauter, G., Söll, I. and Hauptmann, G.** (2011). Multicolor fluorescent in situ hybridization to define abutting and overlapping gene expression in the embryonic zebrafish brain. *Neural Dev.* **6**, 10.

**Lawson, N. D. and Weinstein, B. M.** (2002). In vivo imaging of embryonic vascular development using transgenic zebrafish. *Dev. Biol.* **248**, 307-318.

**Lawson, N. D., Scheer, N., Pham, V. N., Kim, C. H., Chitnis, A. B., Campos-Ortega, J. A. and Weinstein, B. M.** (2001). Notch signaling is required for arterial-venous differentiation during embryonic vascular development. *Development* **128**, 3675-3683.

**Lawson, N. D., Vogel, A. M. and Weinstein, B. M.** (2002). sonic hedgehog and vascular endothelial growth factor act upstream of the Notch pathway during arterial endothelial differentiation. *Dev. Cell* **3**, 127-136.

**Leslie, J. D., Ariza-McNaughton, L., Bermange, A. L., McAdow, R., Johnson, S. L. and Lewis, J.** (2007). Endothelial signalling by the Notch ligand Delta-like 4 restricts angiogenesis. *Development* **134**, 839-844.

**Li, F., Lan, Y., Wang, Y., Wang, J., Yang, G., Meng, F., Han, H., Meng, A., Wang, Y. and Yang, X.** (2011). Endothelial Smad4 maintains cerebrovascular integrity by activating N-cadherin through cooperation with Notch. *Dev. Cell* **20**, 291-302.

**Lindahl, P., Johansson, B. R., Levéen, P. and Betsholtz, C.** (1997). Pericyte loss and microaneurysm formation in PDGF-B-deficient mice. *Science* **277**, 242-245.

**Liu, H., Zhang, W., Kennard, S., Caldwell, R. B. and Lilly, B.** (2010). Notch3 is critical for proper angiogenesis and mural cell investment. *Circ. Res.* **107**, 860-870.

**Manderfield, L. J., High, F. A., Engleka, K. A., Liu, F., Li, L., Rentschler, S. and Epstein, J. A.** (2012). Notch activation of Jagged1 contributes to the assembly of the arterial wall. *Circulation* **125**, 314-323.

**Montero-Balaguer, M., Lang, M. R., Sachdev, S. W., Knappmeyer, C., Stewart, R. A., De La Guardia, A., Hatzopoulos, A. K. and Knapik, E. W.** (2006). The mother superior mutation ablates foxd3 activity in neural crest progenitor cells and depletes neural crest derivatives in zebrafish. *Dev. Dyn.* **235**, 3199-3212.

**Morrow, D., Scheller, A., Birney, Y. A., Sweeney, C., Guha, S., Cummins, P. M., Murphy, R., Walls, D., Redmond, E. M. and Cahill, P. A.** (2005). Notch-mediated CBF-1/RBP-Jkappa-dependent regulation of human vascular smooth muscle cell phenotype in vitro. *Am. J. Physiol.* **289**, C1188-C1196.

**Noseda, M., Fu, Y., Niessen, K., Wong, F., Chang, L., McLean, G. and Karsan, A.** (2006). Smooth Muscle alpha-actin is a direct target of Notch/CSL. *Circ. Res.* **98**, 1468-1470.

**Olson, L. E. and Soriano, P.** (2011). PDGFRβ signaling regulates mural cell plasticity and inhibits fat development. *Dev. Cell* **20**, 815-826.

**Parsons, M. J., Pisharath, H., Yusuff, S., Moore, J. C., Siekmann, A. F., Lawson, N. and Leach, S. D.** (2009). Notch-responsive cells initiate the secondary transition in larval zebrafish pancreas. *Mech. Dev.* **126**, 898-912.

**Peppiatt, C. M., Howarth, C., Mobbs, P. and Attwell, D.** (2006). Bidirectional control of CNS capillary diameter by pericytes. *Nature* **443**, 700-704.

**Proweller, A., Pear, W. S. and Parmacek, M. S.** (2005). Notch signaling represses myocardin-induced smooth muscle cell differentiation. *J. Biol. Chem.* **280**, 8994-9004.

**Que, J., Wilm, B., Hasegawa, H., Wang, F., Bader, D. and Hogan, B. L. M.** (2008). Mesothelium contributes to vascular smooth muscle and mesenchyme during lung development. *Proc. Natl. Acad. Sci. USA* **105**, 16626-16630.

**Rebay, I., Fehon, R. G. and Artavanis-Tsakonas, S.** (1993). Specific truncations of Drosophila Notch define dominant activated and dominant negative forms of the receptor. *Cell* **74**, 319-329.

**Sakata, Y., Xiang, F., Chen, Z., Kiriyama, Y., Kamei, C. N., Simon, D. I. and Chin, M. T.** (2004). Transcription factor CHF1/Hey2 regulates neointimal formation in vivo and vascular smooth muscle proliferation and migration in vitro. *Arterioscler. Thromb. Vasc. Biol.* **24**, 2069-2074.

**Salloway, S. and Hong, J.** (1998). CADASIL syndrome: a genetic form of vascular dementia. *J. Geriatr. Psychiatry Neurol.* **11**, 71-77.

**Santoro, M. M., Pesce, G. and Stainier, D. Y.** (2009). Characterization of vascular mural cells during zebrafish development. *Mech. Dev.* **126**, 638-649.

**Sengillo, J., Winkler, E. A., Walker, C. T., Sullivan, J. S., Johnson, M. and Zlokovic, B. V.** (2013). Deficiency in mural vascular cells coincides with blood-brain barrier disruption in Alzheimer's disease. *Brain Pathol.* **23**, 303-310.

**Siekmann, A. F. and Lawson, N. D.** (2007). Notch signalling limits angiogenic cell behaviour in developing zebrafish arteries. *Nature* **445**, 781-784.

**Stewart, R. A., Arduini, B. L., Berghmans, S., George, R. E., Kanki, J. P., Henion, P. D. and Look, A. T.** (2006). Zebrafish foxd3 is selectively required for neural crest specification, migration and survival. *Dev. Biol.* **292**, 174-188.

**Sweeney, C., Morrow, D., Birney, Y. A., Coyle, S., Hennessy, C., Scheller, A., Cummins, P. M., Walls, D., Redmond, E. M. and Cahill, P. A.** (2004). Notch 1 and 3 receptor signaling modulates vascular smooth muscle cell growth, apoptosis, and migration via a CBF-1/RBP-Jk dependent pathway. *FASEB J.* **18**, 1421-1423.

**Tallquist, M. D., French, W. J. and Soriano, P.** (2003). Additive effects of PDGF receptor beta signaling pathways in vascular smooth muscle cell development. *PLoS Biol.* **1**, E52.

**Thisse, C. and Thisse, B.** (2008). High-resolution in situ hybridization to whole-mount zebrafish embryos. *Nat. Protoc.* **3**, 59-69.

**von Tell, D., Armulik, A. and Betsholtz, C.** (2006). Pericytes and vascular stability. *Exp. Cell Res.* **312**, 623-629.

**Wang, W., Prince, C. Z., Hu, X. and Pollman, M. J.** (2003). HRT1 modulates vascular smooth muscle cell proliferation and apoptosis. *Biochem. Biophys. Res. Commun.* **308**, 596-601.

**Wang, Q., Zhao, N., Kennard, S. and Lilly, B.** (2012). Notch2 and Notch3 function together to regulate vascular smooth muscle development. *PLoS ONE* **7**, e37365.

**Wiens, K. M., Lee, H. L., Shimada, H., Metcalf, A. E., Chao, M. Y. and Lien, C.-L.** (2010). Platelet-derived growth factor receptor beta is critical for zebrafish intersegmental vessel formation. *PLoS ONE* **5**, e11324.

**Wilm, B., Ipenberg, A., Hastie, N. D., Burch, J. B. E. and Bader, D. M.** (2005). The serosal mesothelium is a major source of smooth muscle cells of the gut vasculature. *Development* **132**, 5317-5328.

**Winkler, E. A., Bell, R. D. and Zlokovic, B. V.** (2011). Central nervous system pericytes in health and disease. *Nat. Neurosci.* **14**, 1398-1405.

**Xie, J., Farage, E., Sugimoto, M. and Anand-Apte, B.** (2010). A novel transgenic zebrafish model for blood-brain and blood-retinal barrier development. *BMC Dev. Biol.* **10**, 76.

**Yamanishi, E., Takahashi, M., Saga, Y. and Osumi, N.** (2012). Penetration and differentiation of cephalic neural crest-derived cells in the developing mouse telencephalon. *Dev. Growth Differ.* **54**, 785-800.

**Zaucker, A., Mercurio, S., Sternheim, N., Talbot, W. S. and Marlow, F. L.** (2013). Notch3 Is essential for oligodendrocyte development and vascular integrity in zebrafish. *Dis. Model. Mech.* **6**, 1246-1259.

**Zygmunt, T., Gay, C. M., Blondelle, J., Singh, M. K., Flaherty, K. M., Means, P. C., Herwig, L., Krudewig, A., Belting, H.-G., Affolter, M. et al.** (2011). Semaphorin-PlexinD1 signaling limits angiogenic potential via the VEGF decoy receptor sFlt1. *Dev. Cell* **21**, 301-314.

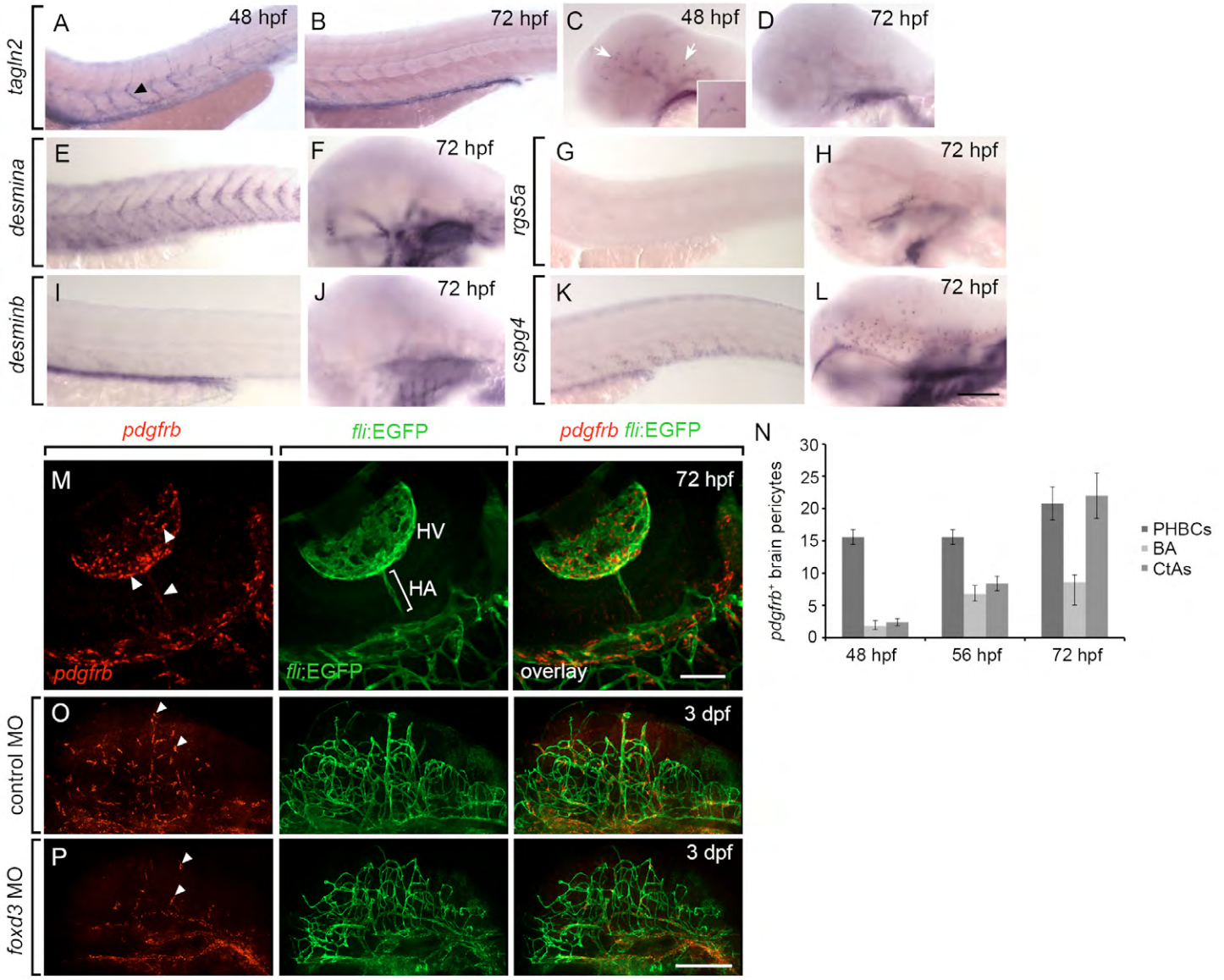


**Fig. S1. Expression patterns of *tagln2* and *pdgfrb* in zebrafish embryos and larvae.** (**A**-**C**) ISH for *tagln2*. (**A**,**B**) *tagln2* expression in trunk vessels at 48 hpf and 72 hpf, respectively. Arrowhead, *tagln2*$^+$ putative mural cell in ISV. (**C**,**D**) *tagln2* expression in brain vasculature at 48 hpf and 72 hpf. Arrow, *tagln2*$^+$ putative brain mural cell. Inset, high magnification view of *tagln2*$^+$ cells in the brain. (**E**-**L**) *desmina*, *desminb*, *rgs5a*, and *cspg4* expression in trunk and brain vasculature at 72 hpf. (**E**,**G**,**I**,**K**) trunk expression. (**F**,**H**,**J**,**L**) brain expression. (**M**) Fluorescent ISH showing *pdgfrb* expression in retinal pericytes at 72 hpf. Arrowheads, *pdgfrb*$^+$ retinal pericytes. (**N**) Quantification of *pdgfrb*$^+$ pericytes associated with different hindbrain vessels at various time points. (**O,P**) *foxd3* MO knock-down caused reduction in *pdgfrb*$^+$ brain pericyte number. (**O**) Control MO-injected 72 hpf larva. (**P**) *foxd3* MO-injected 72 hpf larva. Arrowheads, *pdgfrb*$^+$ brain pericytes. HA, hyaloid artery; HV, hyaloid vessels. Scale bars: (A-L) 0.5 mm, (M-P) 200 µm.

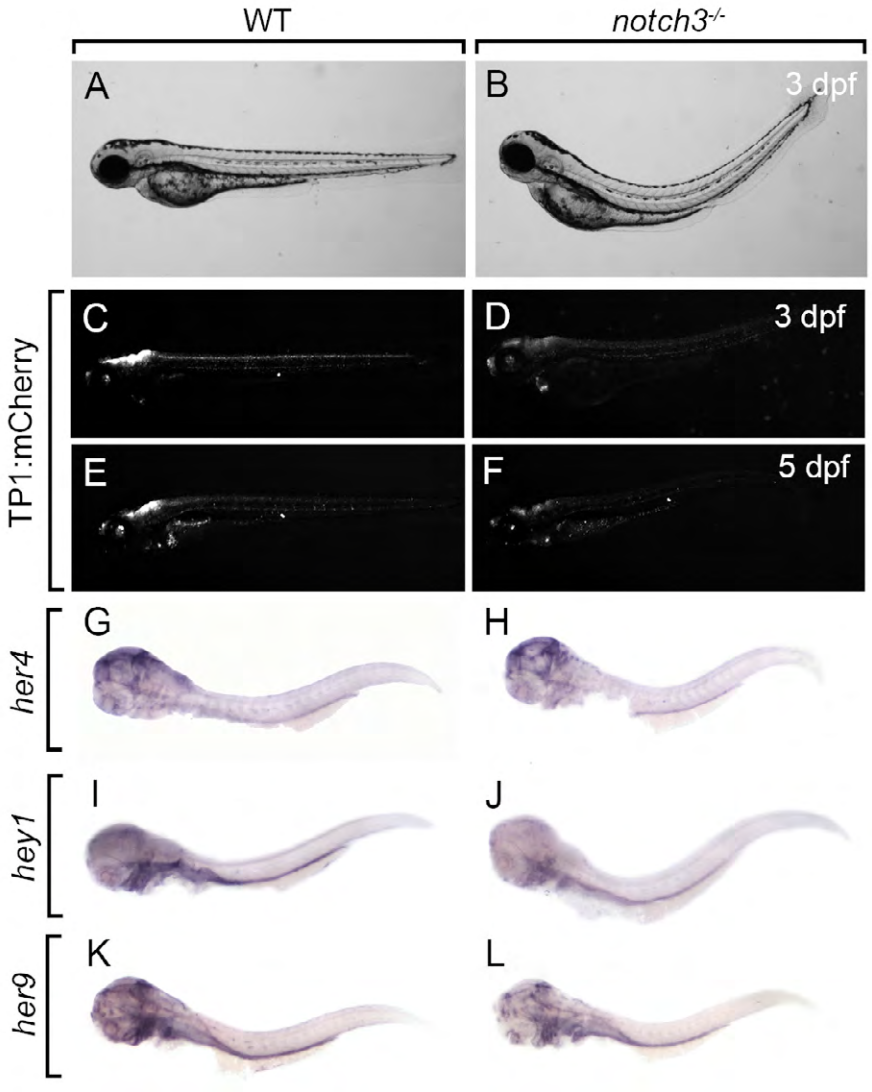


**Fig. S2. *notch3*$^{fh332}$ mutants have reduced Notch signaling activity.** (**A**,**B**) Wild-type and *notch3*$^{fh332}$ mutant larvae showing trunk curvature of the mutant at 3 dpf. (**C-F**) *notch3*$^{fh332}$*; Tg(Tp1bglob:hmgb1-mCherry)* (Tp1:mCherry) mutant larvae showed reduced mCherry expression compared to wild-type siblings at 3 dpf and 5 dpf. (**G,H**) Whole-mount ISH revealed similar *her4.1* expression in *notch3*$^{fh332}$ mutant and wild-type sibling. (**I-L**) *notch3*$^{fh332}$ mutants showed reduced *hey1* and *her9* expression compared to wild-type siblings.

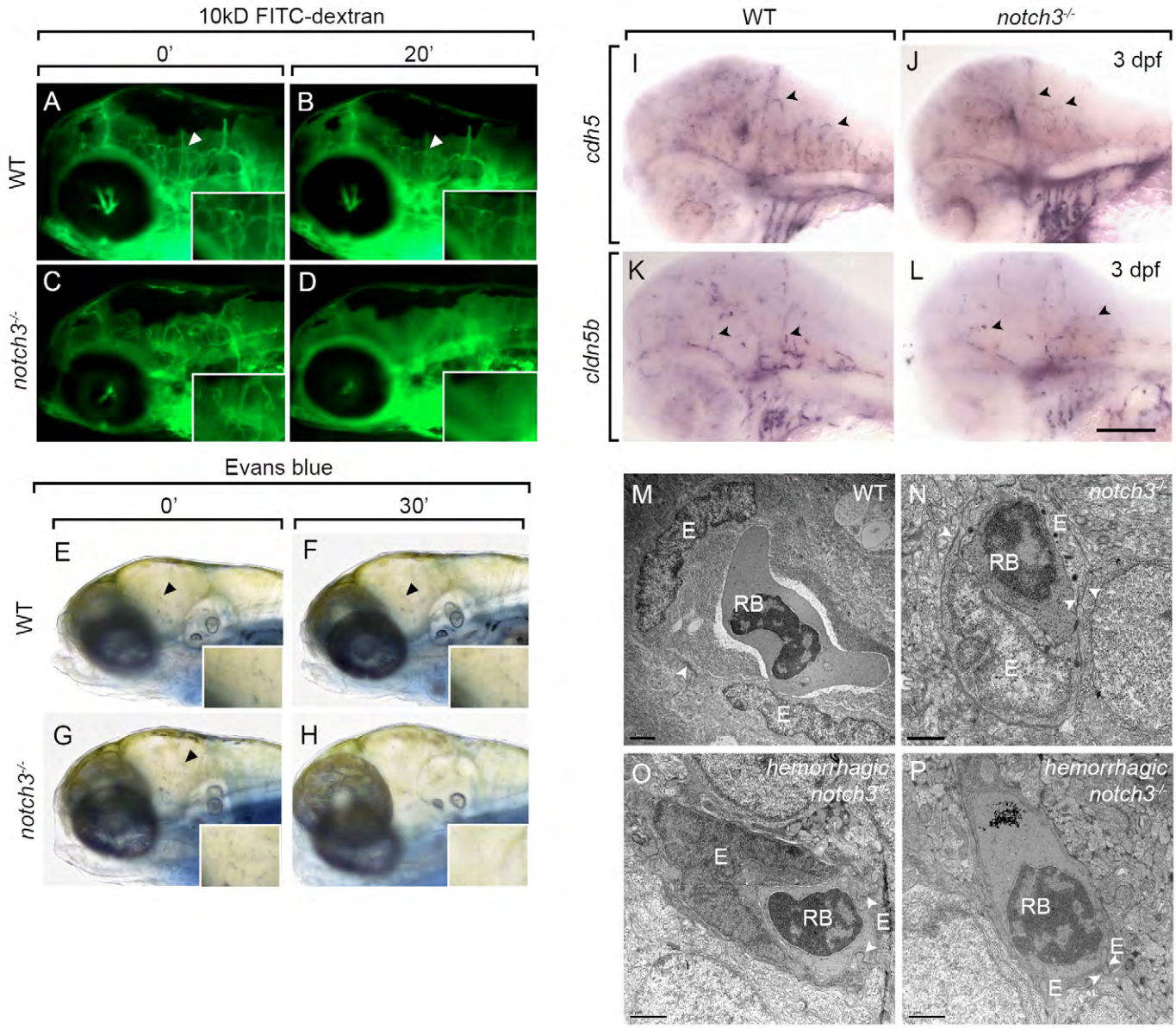


**Fig. S3. Endothelial cell differentiation in *notch3*$^{fh332}$ mutant larvae.** (**A-H**) Representative results of BBB assay in 4 dpf wild-type and mutant larvae using 10KD FITC-dextran and Evans blue dye. Insets, higher magnification view of brain microvessels. (**A-D**) Mutant embryos failed to retain 10KD FITC-dextran in the brain microvessels 20 min after the injection. (**E-H**) Mutant embryos failed to retain Evans blue dye in the brain microvessels 30 min after the injection. (**I-L**) ISH showing *cdh5* and *cldn5b* expression in the brain of 3 dpf wild-type and *notch3*$^{fh332}$ larvae. Arrowheads, endothelial expression of *cdh5* or *cldn5b*. (**M-P**) Electron microscopy images of brain microvessels in 4 dpf wild-type and *notch3*$^{fh332}$ mutant larvae. RB, red blood cell. E, endothelial cell. Arrowheads, endothelial tight junctions. Scale bars: (**I-L**) 250 μm, (**M-P**) 1μm.

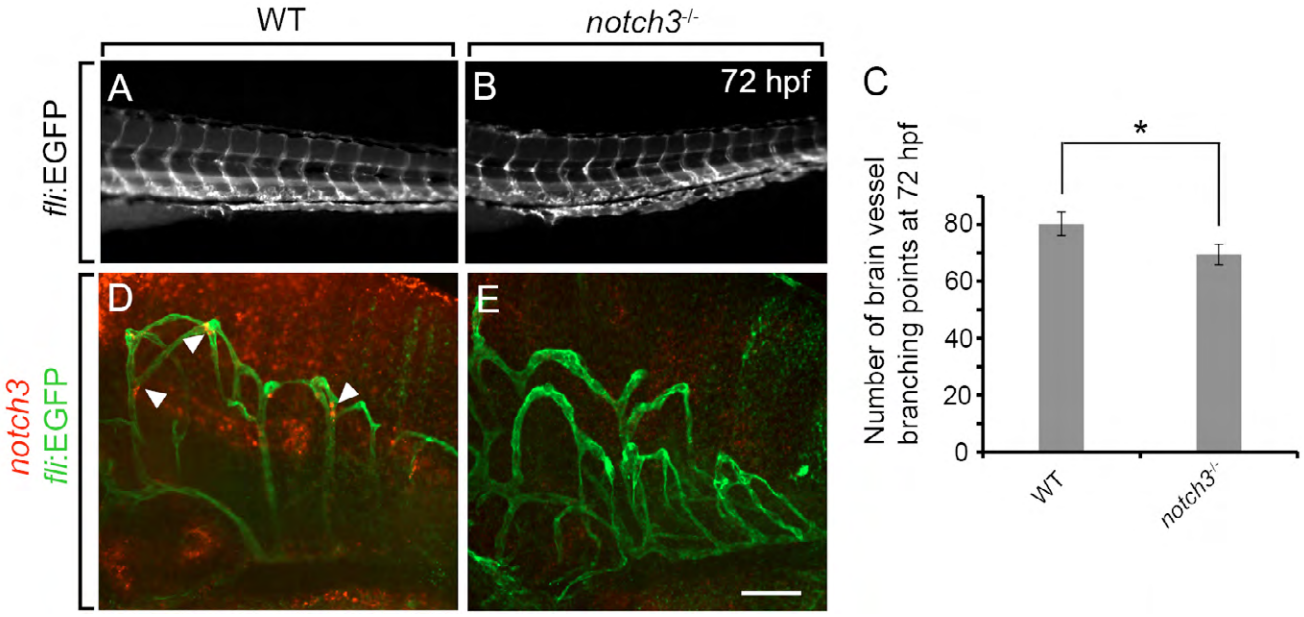


**Fig. S4. Vascular morphogenesis and brain *notch3* expression in *notch3*$^{fh332}$ mutants.** (**A**,**B**) *fli1*:EGFP transgenic reporter expression showing trunk vessels in 72 hpf wild-type and *notch3*$^{fh332}$ mutant larvae. (**C**) Quantification of vessel branch points in the brain of *notch3*$^{fh332}$ mutant and wild-type larvae. (**D**,**E**) Fluorescent ISH showing *notch3* expression in the hindbrain. Pericyte *notch3* expression was largely depleted in the mutant. Arrowheads, *notch3*$^{+}$ pericytes. *$P$<0.01 by Student's 2-tailed t test. Scale bar, 200 µm.

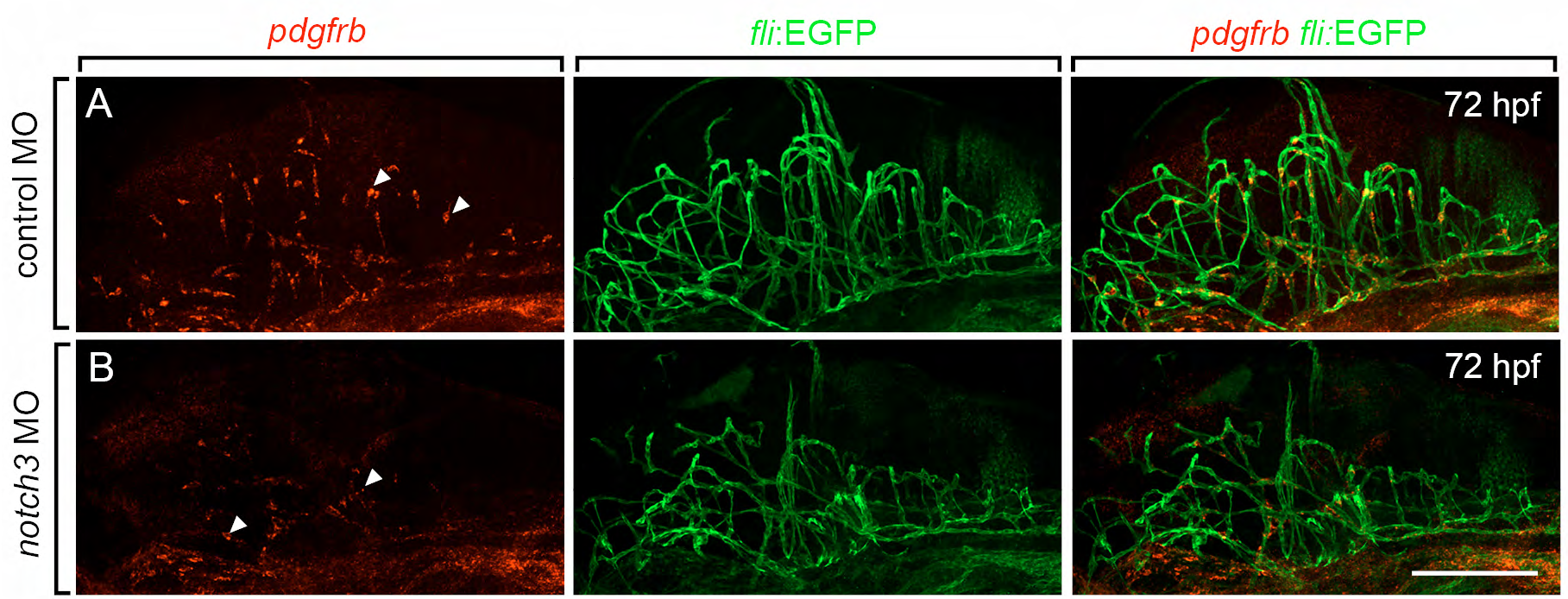


**Fig. S5. *notch3* MO phenocopied the pericyte deficit phenotype in *notch3*$^{fh332}$ mutant larvae.** (**A**,**B**) Fluorescent ISH showing *pdgfrb*$^{+}$ brain pericytes in 72 hpf control and *notch3* MO-injected larvae. Arrowheads, *pdgfrb*$^{+}$ pericytes. Scale bar, 200 μm.

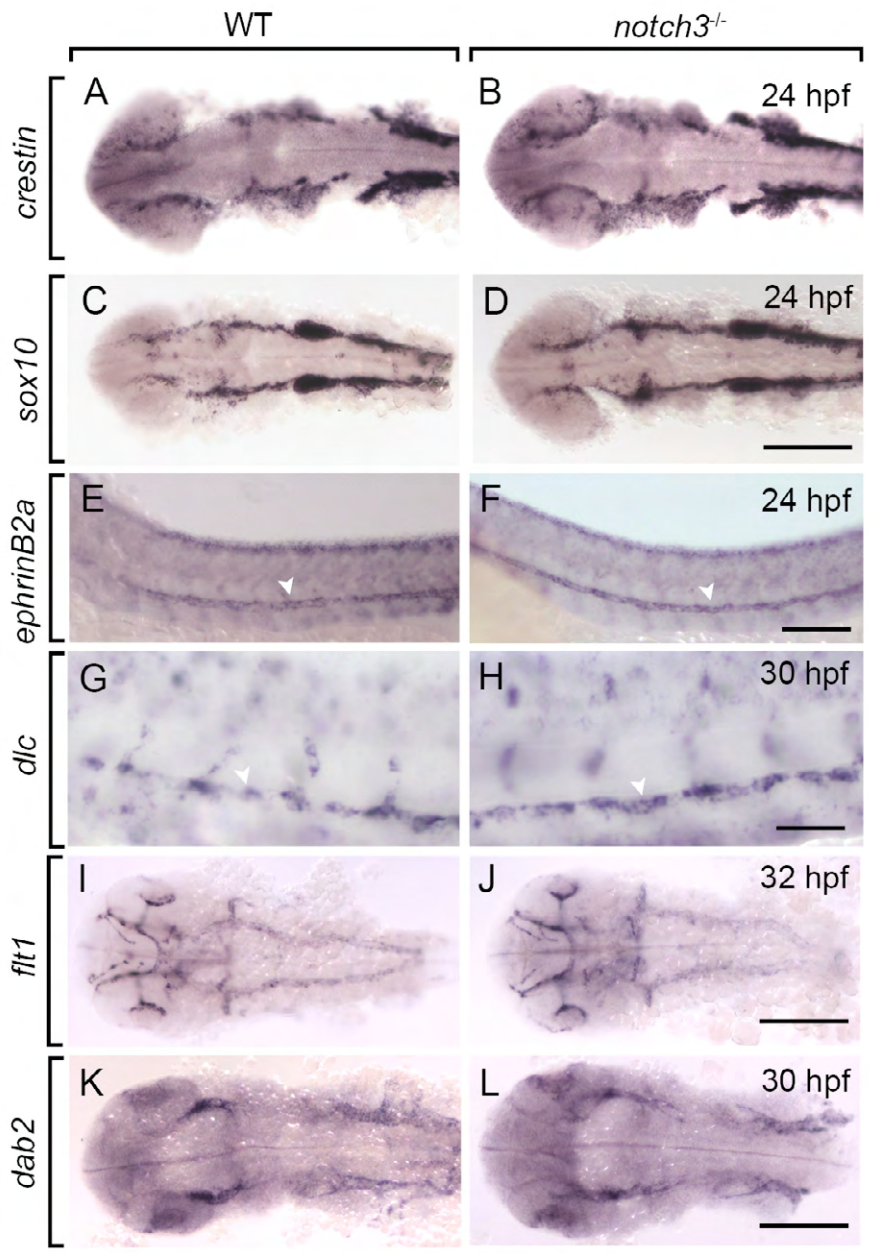


**Fig. S6. Arterial-venous differentiation and neural crest development in *notch3*$^{fh332}$ mutant larvae.** (**A**-**D**) ISH showing *crestin* and *sox10* expression in 24 hpf wild-type and *notch3*$^{fh332}$ mutant larvae. (**E**,**F**) ISH showing *efnb2a* expression in 24 hpf wild-type and *notch3*$^{fh332}$ mutant larvae. (**G**,**H**) ISH showing *dlc* expression in 30 hpf wild-type and *notch3*$^{fh332}$ mutant larvae. Arrowheads, DA. (**I**,**J**) ISH showing *flt1* expression in 32 hpf wild-type and *notch3*$^{fh332}$ mutant larvae. (**K**,**L**) ISH showing *dab2* expression in 30 hpf wild-type and *notch3*$^{fh332}$ mutant larvae. Scale bars: (**A**-**F**) 0.5 mm, (**G**,**H**) 200 µm. (I-L) 0.5mm.

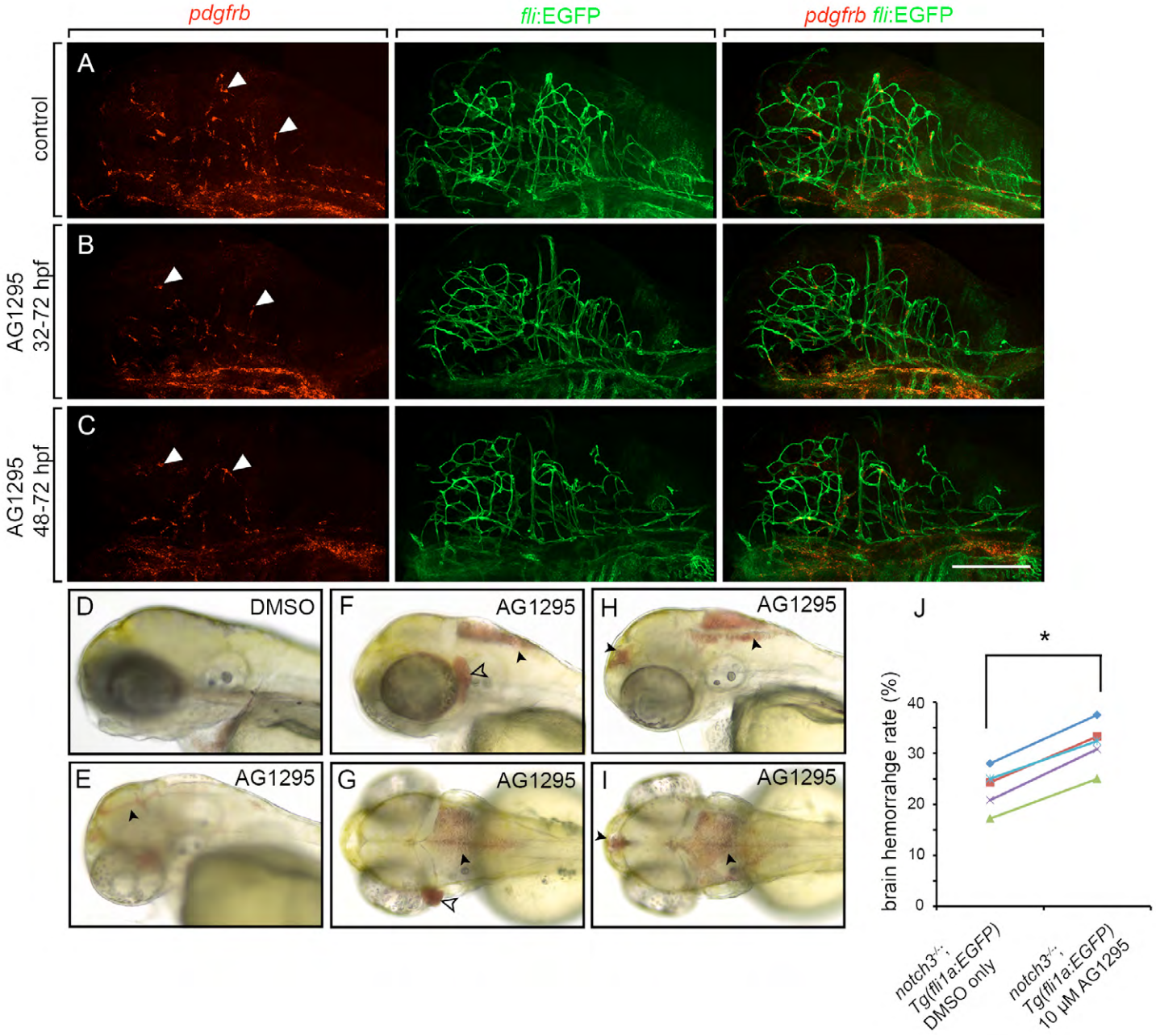


**Fig. S7. Inhibition of Pdgfr-β activity produces a pericyte deficit and brain hemorrahge.** (**A**) *pdgfrb*$^{+}$ brain pericytes in DMSO treated control larvae. (**B**,**C**) Larvae treated with 25 µM AG1295 from 32-72 hpf, and from 48-72 hpf, respectively, showed a reduction in *pdgfrb*$^{+}$ brain pericyte number. Arrowheads, *pdgfrb*$^{+}$ brain pericytes. Scale bar, 200 µm. (**A-C**) All images show confocal projections of whole brains, viewed from lateral. (**D-I**) Brain hemorrhage in AG1295 treated zebrafish larvae. (**D**) DMSO treated control at 3 dpf. (**F-I**) 25µm AG1295 treated larva at 3 dpf. (**E**,**F**,**H**) Lateral views. (**G**,**I**) Dorsal views of (**F**,**H**), respectively. (**J**) *notch3*$^{fh332}$ homozygous mutants showed a more penetrant hemorrhage phenotype when treated with 10 µM AG1295 ($n$=5, *$P$<0.05, by paired t-test). Arrowheads, blood pooling at the brain ventricle; open arrowhead, blood pooling behind the eye.

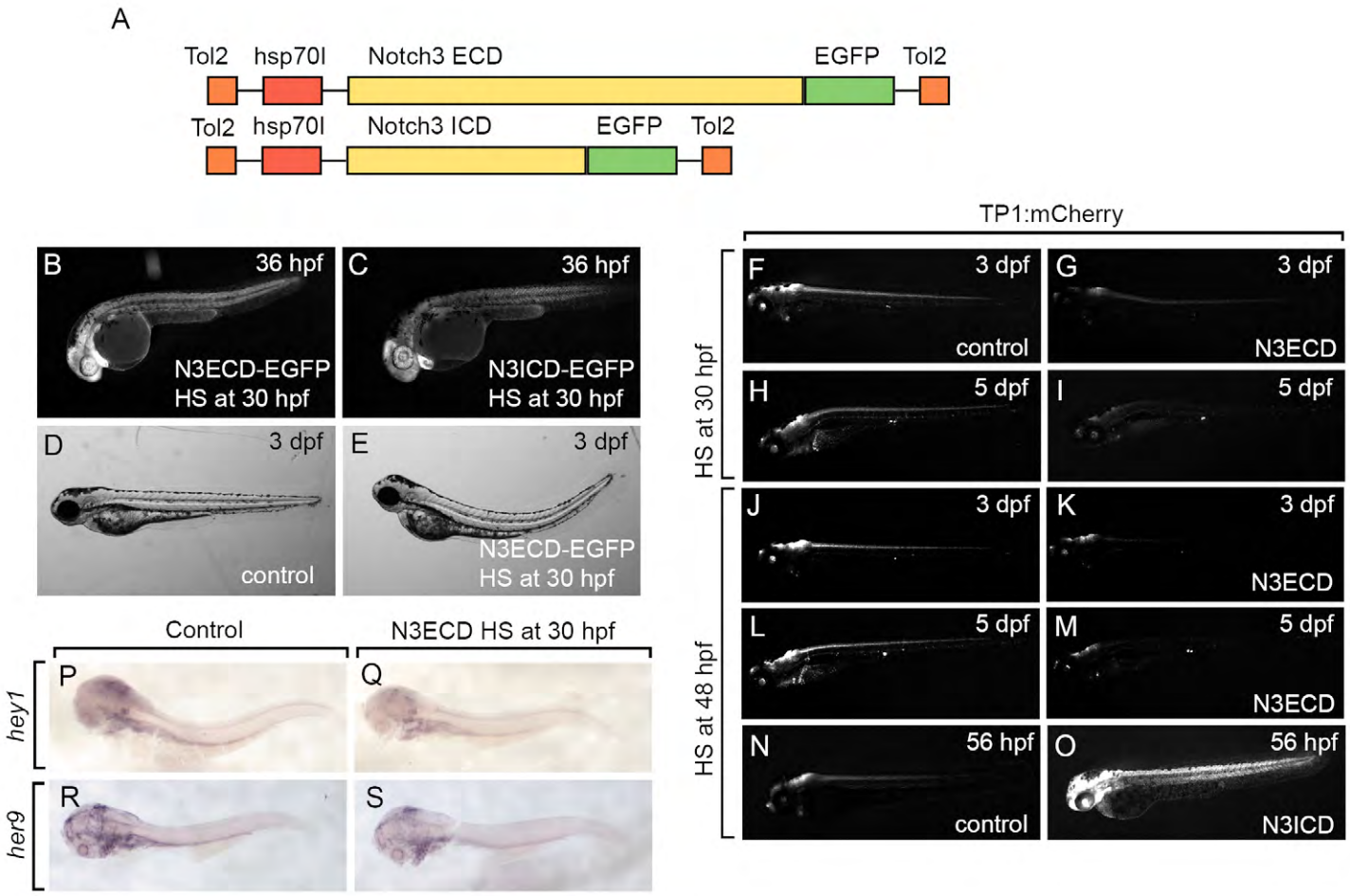


**Fig. S8. Organization and transgene expression for *Tg(hsp70I:Notch3ECD-EGFP)* and *Tg(hsp70I:Notch3ICD-EGFP)* transgenic constructs.** (**A**) Diagram depicting the organization of *Tg(hsp70I:Notch3ECD-EGFP)* and *Tg(hsp70I:Notch3ICD-EGFP)* transgenic constructs. (**B**,**C**) Heat shock of *Tg(hsp70I:Notch3ECD-EGFP)* embryos (**B**) and *Tg(hsp70I:Notch3CD-EGFP)* embryos (**C**) at 30 hpf induced robust EGFP expression. (**D**,**E**) Heat shock of *Tg(hsp70I:Notch3ECD-EGFP)* embryos at 30 hpf resulted in trunk curvature at 3 dpf. (**F-M**) Heat shock of *Tg(hsp70I:Notch3ECD-EGFP)*; *Tg(Tp1bglob:hmgb1-mCherry)* embryos at 48 hpf or 30 hpf caused significant reduction in mCherry intensity at 3 dpf and 5 dpf. (**N**,**O**) Heat shock of *Tg(hsp70I:Notch3ICD-EGFP)*; *Tg(Tp1bglob:hmgb1-mCherry)* embryos at 48 hpf resulted in significantly increased mCherry fluorescent intensity at 56 hpf. (**P-S**) *Tg*(*hsp70I:N3ECD-EGFP)* larvae heat-shocked at 30 hpf showed reduced *heyl* and *her9* expression compared to control group.

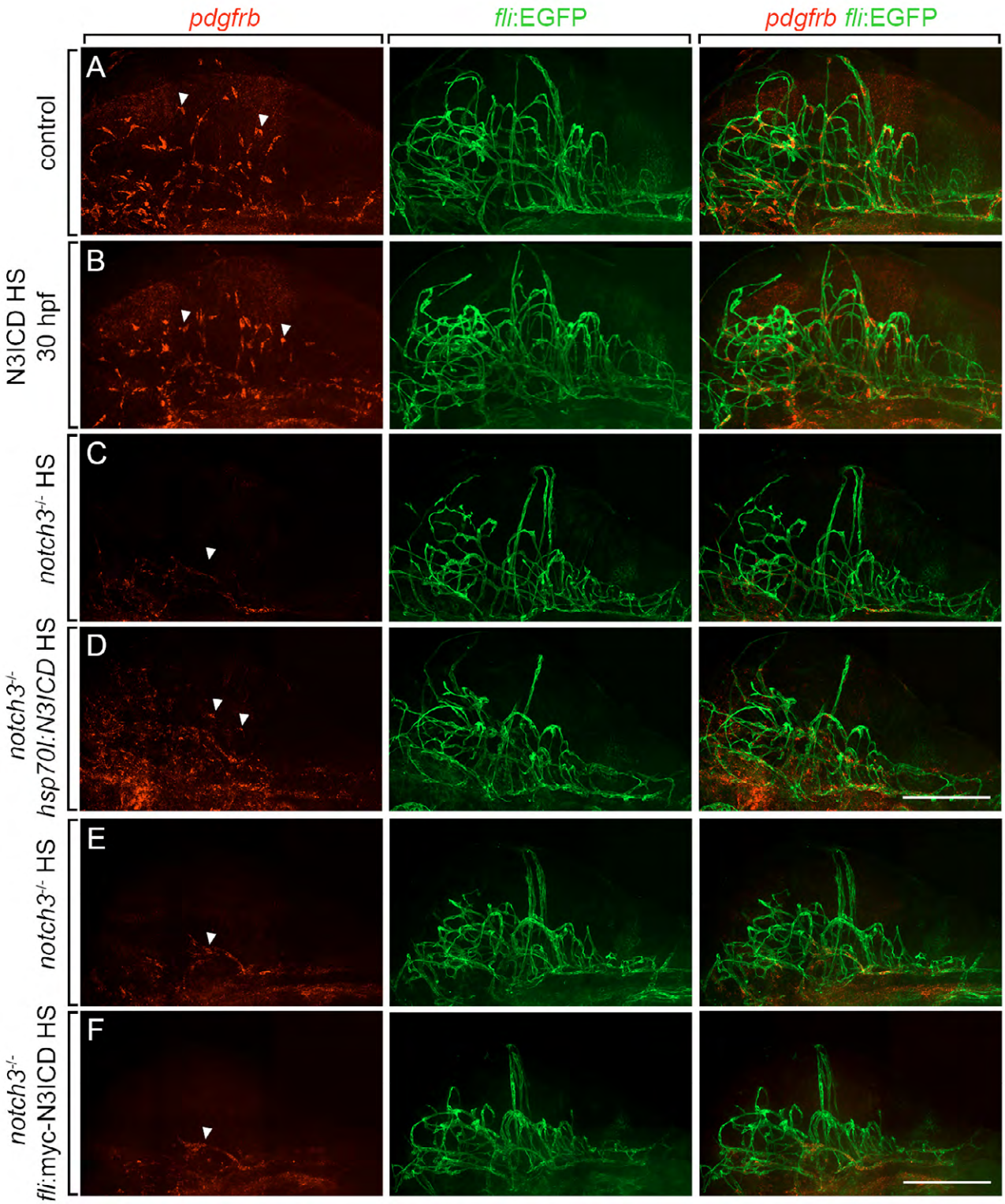


**Fig. S9. Notch3 is insufficient to induce ectopic brain pericyte specification and forced Notch3ICD expression in the endothelium failed to rescue the pericyte deficit in *notch3*$^{fh332}$ larvae**. (**A**,**B**) Heat shock of *Tg(hsp70I:Notch3ICD-EGFP)* embryos at 30 hpf did not result in increase of brain pericyte number at 72 hpf. (**A**) Non-transgenic control larvae. (**B**) *Tg*(*hsp70I:N3ICD-EGFP)* larva heat shocked at 30 hpf. (**C**,**D**) Transient N3ICD overexpression partially rescued the brain pericyte deficit phenotype in *notch3*$^{fh332}$ mutant larvae at 72 hpf. (**C**) *notch3*$^{fh332}$ mutant mock-injected control. (**D**) *notch3*$^{fh332}$ mutant injected with *hsp70I:N3ICD-GFP* construct and heatshocked at 48 hpf. (**E**,**F**) Transient *N3ICD* expression in endothelial cells failed to rescue the brain pericyte deficit phenotype in *notch3*$^{fh332}$ mutant larvae. (**E**) *notch3*$^{fh332}$ mutant mock-injected control. (**F**) *notch3*$^{fh332}$ mutant injected with *fli1:myc-Notch3ICD* construct and heat shocked at 48 hpf. Arrowheads, *pdgfrb*$^{+}$ brain pericytes. Scale bar, 200 μm.

**Table S1. Brain hemorrahge phenotype in *notch3*$^{fh332}$ larvae, *notch3* MO treated larvae, *foxd3* MO treated larvae, and AG1295 treated larvae.**

| Genotype or treatment | Hemorrahge rate |
|---|---|
| *notch3*$^{fh332}$ | 10% (n = 30) |
| | 6.25% (n = 32) |
| | 12.5% (n = 40) |
| | 19.5% (n= 87) |
| *notch3*$^{fh332}$;*Tg(fli1a:EGFP)* | 25% (n = 56) |
| | 24.4% (n = 45) |
| | 19.4% (n = 31) |
| | 28.9% (n = 76) |
| | 12.5% (n = 48) |
| control MO | 0 (n = 56) |
| | 1.4% (n = 72) |
| | 0 (n = 34) |
| *notch3* MO | 33.3% (n = 66) |
| | 31.6% (n = 57) |
| | 42.2% (n = 45) |
| AB; 25 µM AG1295 30 hpf to 72 hpf | 8.6% (n = 35) |
| | 10.7% (n = 28) |
| AB; 25 µM AG1295 48 hpf to 72 hpf | 4.8% (n =21) |
| | 10.8% (n = 37) |
| *Tg(fli1a:EGFP)* 25 µM AG1295 30 hpf to 72 hpf | 25% (n =60) |
| | 23.1% (n= 39) |
| | 31.0% (n =42) |
| *Tg(fli1a:EGFP)* 25 µM AG1295 48 hpf to 72 hpf | 16.7% (n =30) |
| | 19.3% (n = 31) |
| | 25% (n =20) |
| control MO | 0 (n = 48) |
| | 0 (n = 52) |
| | 0 (n = 63) |
| *foxd3* MO | 15.8% (n = 76) |
| | 11.1% (n = 63) |
| | 6.25% (n= 64) |
| *notch3*$^{fh332}$;*Tg(fli1a:EGFP)* raised at 28°C | 23.5% (n = 34) |
| | 18.8% (n = 32) |
| | 24.1% (n=29) |
| *notch3*$^{fh332}$;*Tg(fli1a:EGFP)* raised at 32°C | 55.6% (n = 36) |
| | 50% (n = 36) |
| | 66.7% (n=27) |

| | |
|---|---|
| *notch3*$^{fh332}$ ;*Tg(fli1a:EGFP)*<br>DMSO only, 30 hpf to 72 hpf | 28% (n = 25) |
| | 24.3% (n =37) |
| | 17.2% (n=29) |
| | 20.8% (n=24) |
| | 25% (n=28) |
| *notch3*$^{fh332}$;*Tg(fli1a:EGFP)*<br>10 µM AG1295 30 hpf to 72 hpf | 37.5% (n = 48) |
| | 33.3% (n = 27) |
| | 25% (n=32) |
| | 30.8% (n=26) |
| | 32.4% (n=34) |